Supplementary Information

The Convergence of DNA Nanotechnology and Polymer Chemistry to 'Synthesize' Nanopolymers with Branching Architectures

Tianyun Cai[1], Qianlin Cai[1], Jiaping Lin[1], and Liangshun Zhang[1]*

[1] *Shanghai Key Laboratory of Advanced Polymeric Materials, School of Materials Science and Engineering, East China University of Science and Technology, Shanghai 200237, China*

*E-mail: zhangls@ecust.edu.cn

This PDF file includes:

S1. Coarse-grained model and sequence of DNA strands

S1.1 Coarse-grained model

The coarse-grained DNA model proposed in the Travesset's group is extended to study the hierarchically programmable coassembly of DNA-based multicomponent mixtures, [S1-S2] which consist of bivalent DNA-functionalized nanoparticles (designated as DNA-NPs **v**) and a diverse range of DNA molecules. The coarse-grained model of bivalent nanoparticles grafted by two DNA strands is illustrated in Figure S1a. The nanoparticles with radius R are represented by spherically symmetric rigid body with a fixed number of beads on their surface. DNA strands attached onto the opposite poles of nanoparticles consist of spacers and stickers with size σ. The sticker bead has additional structures (i.e., two protection beads and one sticky bead with size 0.6σ), which are used to mimic the directional hydrogen bonds between complementary base pairs (i.e., A-T and C-G). The coarse-grained model of DNA molecules **y** for the construction of branch-shaped motif **Y** is illustrated in Figure S1b. The linear structure of DNA molecule **y** has two stickers for the hybridization of various DNA molecules in the course of the construction of motif **Y** as well as branch-shaped nanopolymers. In addition, the highly flexible spacer is incorporated into the DNA molecules **y**. For simplicity, only the sticker beads are included in the DNA molecules of stopper **s** and linkers **l**, which are illustrated in Figure S1c.

The DNA strands are built from harmonically bonded beads via the harmonic spring potential given by

$$U_{bond}(r) = \frac{1}{2}k_s(r - r_0)^2 \qquad \text{(Eq. S1)}$$

where r denotes the distance between two beads, $r_0 = 0.84\sigma$ and $k_s = 330\varepsilon/\sigma^2$. The harmonic angle potential is used to enhance the stiffness of DNA strands

$$U_{angle}(\theta) = \frac{1}{2}k_\theta(\theta - \theta_0)^2 \qquad \text{(Eq. S2)}$$

where ϑ represents the harmonic angle between three consecutive beads, $\vartheta_0 = \pi$ and $k_\theta = 30\varepsilon/rad^2$. The similar potentials are applied to three additional beads attached onto each sticker bead. For the spacer beads of DNA molecules, k_θ is set to zero.

The interactions between complementary sticky beads (i.e., A-T and C-G) are described by the shifted Lennard-Jones potential

$$U(r) = 4\varepsilon_{bp}\left[\left(\frac{\sigma}{r}\right)^{12} - \left(\frac{\sigma}{r}\right)^{6}\right] \qquad \text{(Eq. S3)}$$

where $\varepsilon_{bp} = 10\varepsilon$ is the characteristic attraction strength between complementary base pairs and the cut-off radius is set as $r_c = 2.75\sigma$. The interactions between any other pairs of beads are modeled by the purely repulsive Weeks-Chandler-Andersen potential with cut-off radius $r_c = 2^{1/6}\sigma$

$$U(r) = 4\varepsilon\left[\left(\frac{\sigma}{r}\right)^{12} - \left(\frac{\sigma}{r}\right)^{6}\right] \qquad \text{(Eq. S4)}$$

The coarse-grained molecular dynamics simulations are performed on Graphics

Processing Units with the HOOMD-Blue package under the NVT ensemble. [S3] Rigid body dynamics is introduced to enforce the spherical shape of nanoparticles. [S4] Periodic boundary conditions are applied to the simulated boxes. All beads with equal mass m are placed in a cubic box, where the distance and size are scaled by the length unit σ. In converting to real units, the physical length scale σ has a value of ~ 2.0 nm and the nanoparticle radius $R = 3\sigma$ ~ 6.0 nm. [S5] One sticker bead corresponds to 3 ~ 7 bases in experiments. The temperature of system is expressed in terms of the reduced temperature $T^* = k_BT/\varepsilon$. A time step is chosen to be $\Delta t = 0.001\tau$, where $\tau = \sqrt{m\sigma^2/\varepsilon}$ ~ 40.0 ps is the time unit (m ~ 990 amu = 1.6×10^{-24} kg and $\varepsilon = k_BT = 4.1\times10^{-21}$ J at T = 298 K). Each simulation starts from independently initial configurations of building units. The movement trajectories are visualized by VMD. [S6] All data are averaged over five independent runs.

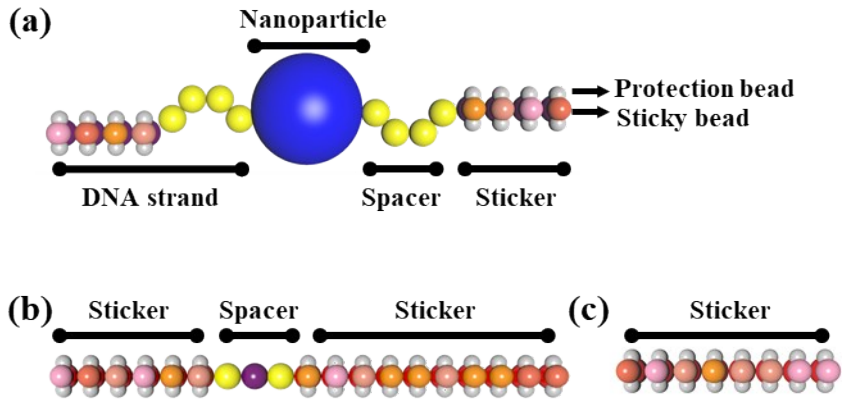

Fig. S1: (a) Coarse-grained model of bivalent DNA-functionalized NPs v. The DNA strands contain the spacer and sticker beads. Each sticker bead is decorated with one sticky bead and two protection beads. (b) Coarse-grained model of DNA molecule **y**. *(c) Coarse-grained model of DNA stoppers* **s** *or linkers* **l**.

S1.2 Sequences of DNA strands

The coarse-grained model of DNA strands facilitates large-scale simulations of programmable coassembly of DNA-based multicomponent mixtures for the construction of branching nanopolymers such as star and graft architectures. As illustrated in Figure 1 of the main text, the star nanopolymers are comprised of branch-shaped motif **Y** as core, end-capped linear prepolymers **V** as arms, and linkers **l** for the connection of core and arms. Correspondingly, the sequences of DNA strands and their hybridization are schematically illustrated in Figure S2. The branch-shaped motif **Y** consists of three distinct DNA molecules $\mathbf{y}_i$ (i = 1, 2 and 3). Each DNA molecule $\mathbf{y}_i$ comprises two 6-base-long stems with complementary sequences that facilitate the ligation with other DNA molecules $\mathbf{y}_i$, and one 4-base-long sticky end that enables the ligation with linker **l**. The prepolymers of NPs consist of three components (i.e., bivalent DNA-NPs **v**, linkers **l** and stopper **s**). The DNAs grafted onto the NPs have complementary sequences, which program the NPs to polymerize into one-dimensional chains. The DNA molecules **s** act as stoppers to suppress the polymerization of DNA-NPs. Note that the DNA linkers **l** have two domains: the complementary sequence of DNA-NPs for stopping the polymerization of DNA-NPs and the complementary sequence of sticky ends of

DNA molecules $\mathbf{y}_i$ for the connection between the motifs **Y** and prepolymers **V**.

Figure S3 schematically illustrates the sequences of DNA strands and their hybridization for the construction of graft nanocopolymers. The sequences of DNA molecules $\mathbf{y}_i$ for the stems of branch-shaped motifs **Y** are the same as the case of star nanopolymers, but two of the sticky ends are complementary with the linkers **l'**. Thus, the branch-shaped motifs **Y** in the presence of linkers **l'** polymerize into the backbones **B** of graft nanocopolymers. The end-capped prepolymers **V** are grafted onto the backbones via the hybridization between the sticky ends of motifs **Y** and the linkers **l**. Similarly, the sequences of DNA molecules $\mathbf{y}_i$ for the cores of miktoarm and four-arm star nanopolymers are shown in Figure S4.

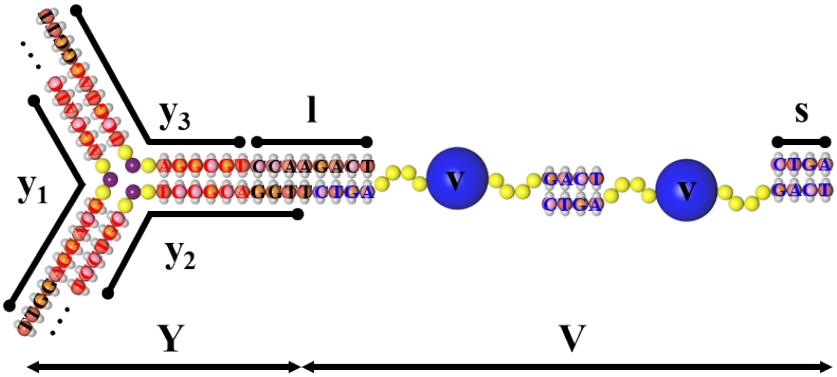

Fig. S2: Sequence and hybridization of DNA strands (i.e., DNA molecules $\mathbf{y}_i$*, linkers* **l***, DNA-NPs* **v** *and stoppers* **s***) for the construction of star nanopolymers. Note that only one arm of star nanopolymers is shown and all the DNA molecules* $\mathbf{y}_i$ *have the same sequences of sticky ends.*

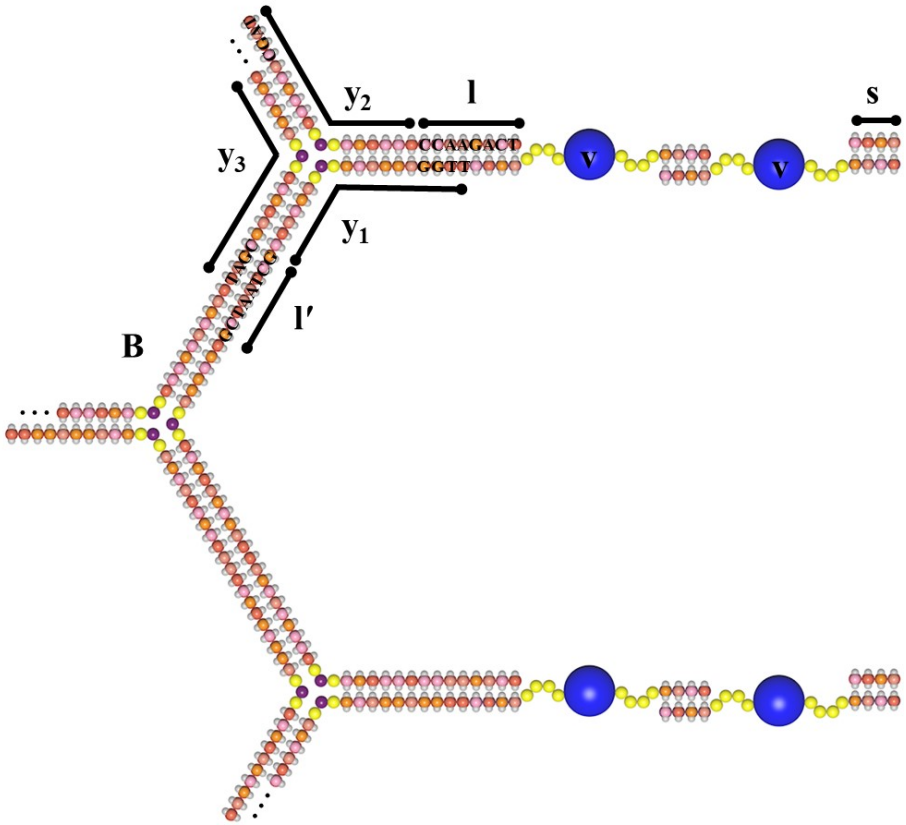

Fig. S3: Sequence and hybridization of DNA strands (i.e., DNA molecules $\mathbf{y}_i$*, linkers* **l** *and* **l'***, DNA-*

NPs **v** *and stoppers* **s***) for the construction of graft nanocopolymers. Note that the DNA molecules* $\mathbf{y_2}$ *and* $\mathbf{y_3}$ *have the same sequences of sticky ends for the polymerization of branch-shaped motifs* **Y** *into the backbones* **B** *of graft nanocopolymers. Only the hybridization sequences of DNA linkers* **l** *and* **l**′ *are shown.*

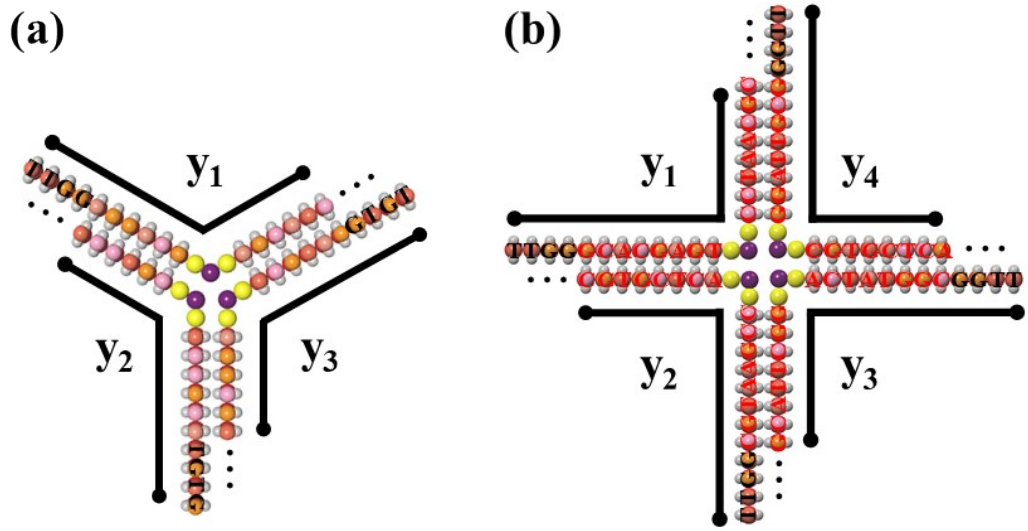

Fig. S4: Sequence and hybridization of DNA strands for the construction of (a) miktoarm and (b) four-arm star nanopolymers. Note that only the cores of star nanopolymers are shown.

S2. Theoretical model of coassembly kinetics of DNA-based multicomponent mixtures

In our previous works, [S7,S8] we used the polymerization kinetics model in the field of polymer chemistry to quantitatively understand the programmable self-assembly of bivalent DNA-NPs, which is used to build upon linear nanopolymers through the hybridization/dehybridization of DNA strands. Herein, we further extend the polymerization kinetics model to capture the assembly/disassembly kinetics of DNA-based multicomponent systems in the course of the formation of nonlinear nanopolymers (e.g., the growth dynamics of nanopolymers, type and distribution of coassembled productions), and compare the simulation results with the theoretical predictions of polymerization kinetics. It is assumed that the assembly and disassembly rates remain constant and are independent upon the length of coassemblies (i.e., the Flory's assumptions of equal reactivity). [S9-S10]

S2.1 Prepolymerization of DNA-NPs and DNA molecules

We first provide the definitions of variables in the formulations of the prepolymerization model of bivalent DNA-NPs. Unlike the simple system considered previously, [S8,S9] the current system contains three types of components for the construction of prepolymers **V** (e.g., bivalent DNA-NPs **v**, monovalent DNA molecules of stoppers **s** and linkers **l** herein). The initial concentration is defined as $c_{v(s,\,l)0} = n_{v(s,\,l)}/L^3$, where $n_{v(s,\,l)}$ is the initial number of DNA-NPs **v** (stoppers **s** or linkers **l**) and L is the size of simulation boxes. The concentration at the assembly time t is denoted by c. The prepolymerization process can be described by a series of hybridization reactions. In particular, two ends of bivalent DNA-NPs are respectively designated as # and *, and their hybridization results in the formation of v-v bonds. In the course of prepolymerization, the nanopolymers can be end-capped by both stoppers **s** and linkers **l**, which are designated as the letter of 'e' in the hybridization reaction listed below.

Reaction 1: For the homopolymerization of bivalent DNA-NPs **v**

$$-v\# + *v- \underset{k_{d,v-v}}{\overset{k_{a,v-v}}{\Longleftrightarrow}} -v-v-$$

One can write the following second-order kinetic equation of the concentration $c_{v\text{-}v}$ of v-v bonds

$$\begin{aligned}\frac{dc_{v-v}}{dt} &= k_{a,v-v}c_{v,free}^{2} - k_{d,v-v}c_{v-v} \\ &= k_{a,v-v}\left(c_{v0} - c_{v-v} - c_{v-e}/2\right)^2 - k_{d,v-v}c_{v-v}\end{aligned} \qquad \text{(Eq. S5)}$$

where $k_{a,v\text{-}v}$ and $k_{d,\,v\text{-}v}$ are respectively the assembly and disassembly rate constants of prepolymer chains due to the hybridization and dehybridization of complementary DNA strands. The concentrations of free # and * ends of bivalent DNA-NPs in the polymerization reaction remain the same value due to the simultaneous consumption of complementary DNA strands (i.e., $c_{v,\,free} = c_{v\#,\,free} = c_{v*,\,free}$). The parenthesis is the concentration of free ends of DNA strands. Note that the initial concentration of bivalent DNA-NPs is given by c_{v0}.

Reaction 2: For the hybridization reactions of the free * and # ends of prepolymer chains with the DNA stoppers **s** and linkers **l**. Specifically, such reactions include (a) the hybridization between * ends and stoppers **s** and (b) the hybridization between # ends and linkers **l**. In the prepolymerization stage, both hybridization events lead to the formation of end-capped prepolymers

$$-v*+s \underset{k_{d,v-s}}{\overset{k_{a,v-s}}{\Longleftrightarrow}} -v-s$$

$$-v\#+l \underset{k_{d,v-l}}{\overset{k_{a,v-l}}{\Longleftrightarrow}} -v-l$$

The following kinetic equations are given by

$$\frac{dc_{v-s}}{dt} = k_{a,v-s}c_{v,free}c_{s,free} - k_{d,v-s}c_{v-s}$$

$$\frac{dc_{v-l}}{dt} = k_{a,v-l}c_{v,free}c_{l,free} - k_{d,v-l}c_{v-l}$$

We introduce $c_{v\text{-}e} = c_{v\text{-}s} + c_{v\text{-}l}$ and the rate constants in the above reactions are assumed to be identical (e.g., $k_{a,v\text{-}s} = k_{a,v\text{-}l} = k_{a,v\text{-}e}$, $k_{d,v\text{-}s} = k_{d,v\text{-}l} = k_{d,v\text{-}e}$). In consideration of the constraints $c_{l,\,free} = c_{s,\,free} = c_{e,free}/2$ and $c_{v\text{-}s} = c_{v\text{-}l} = c_{v\text{-}e}/2$, the kinetic equation of $c_{v\text{-}e}$ is re-written as

$$\begin{aligned}\frac{dc_{v-e}}{dt} &= 2k_{a,v-e}c_{v,free}c_{l,free} - k_{d,v-e}c_{v-e} \\ &= k_{a,v-e}\left(c_{v0} - c_{v-v} - c_{v-e}/2\right)\left(c_{e0} - 2c_{e-e} - c_{v-e}\right) - k_{d,v-e}c_{v-e}\end{aligned} \quad \text{(Eq. S6)}$$

where the second parenthesis is the concentration of complementary sequence of stopper **s** and linkers **l**. The initial value is given by $c_{e0} = 2c_{s0}$.

Reaction 3: For the dimerization between stoppers **s** and linkers **l**

$$s + l \underset{k_{d,s-l}}{\overset{k_{a,s-l}}{\Longleftrightarrow}} s-l$$

is described by the second-order kinetic equation

$$\frac{dc_{s-l}}{dt} = k_{a,s-l}c_{s,free}c_{l,free} - k_{d,s-l}c_{s-l}$$

where $k_{a,s\text{-}l}$ and $k_{d,s\text{-}l}$ are respectively the assembly and disassembly rate constants of DNA molecules **s** and **l**. As mentioned in Reaction 2, both the stoppers and linkers can inhibit the growth of nanopolymers. The equation can be re-written as

$$\begin{aligned}\frac{dc_{e-e}}{dt} &= k_{a,e-e}c_{e,free}^{2}/4 - k_{d,e-e}c_{e-e} \\ &= k_{a,e-e}\left(c_{e0} - 2c_{e-e} - c_{v-e}\right)^2/4 - k_{d,e-e}c_{e-e}\end{aligned} \quad \text{(Eq. S7)}$$

It should be mentioned that in absence of DNA molecules **s** and **l**, Eq. S5 can be simplified as

$$\frac{dc_{v-v}}{dt} = k_{a,v-v}(c_{v0} - c_{v-v})^2 - k_{d,v-v}c_{v-v} \quad \text{(Eq. S8)}$$

For the control simulations (i.e., c_{s0} = c_{l0} = 0.0), fitting of Eq. S8 to the simulation date of $c_{v\text{-}v}$ can yield the assembly and disassembly rate constants $k_{a,v\text{-}v}$ and $k_{d,v\text{-}v}$ of DNA-NPs. These values of $k_{a,v\text{-}v}$ and $k_{d,v\text{-}v}$ are used to fit the variations of $c_{v\text{-}v}$, $c_{v\text{-}e}$ and $c_{e\text{-}e}$ in terms of the assembly time *t*. In this manner, we deduce the remaining rate constants $k_{a,v\text{-}e}$ and $k_{d,v\text{-}e}$ as well as $k_{a,e\text{-}e}$ and $k_{d,e\text{-}e}$.

The concentrations *c* of v-v, v-e and e-e bonds can be used to deduce the number-average degree M_n of polymerization and the number fractions *P* of distinct prepolymers. The deduction of these quantities is as follows: The number n_x of nanopolymers containing *x* DNA-NPs (i.e., (*x*-1) v-v bonds) is given by

$$n_x = n_{x,0e} + n_{x,1e} + n_{x,2e} \quad \text{(Eq. S9)}$$

where $n_{x,0e}$ is the number of nanopolymers with active ends, $n_{x,1e}$ is the number of one-end-capped nanopolymers, and $n_{x,2e}$ is the number of both-end-capped nanopolymers. The value of n_x is written as

$$n_x/n_v = f_{v\text{-}v}^{(x-1)} f_{v,free}^2 + 2 f_{v\text{-}v}^{(x-1)} f_{v,free} f_{v\text{-}e} + f_{v\text{-}v}^{(x-1)} f_{v\text{-}e}^2 = f_{v\text{-}v}^{(x-1)}(f_{v,free} + f_{v\text{-}e})^2 \quad \text{(Eq. S10)}$$

where $f_{v\text{-}v} = c_{v\text{-}v}/c_{v0}$ is the fraction of grafted DNA strands reacted with the complementary DNA strands to form the v-v bonds, $f_{v,free} = (c_{v0} - c_{v\text{-}v} - c_{v\text{-}e}/2)/c_{v0}$ is the fraction of unreacted DNA strands, and $f_{v\text{-}e} = c_{v\text{-}e}/2c_{v0}$ is the fraction of DNA strands reacted with the DNA molecules **s** or **l** to form the v-e bonds (i.e., capped ends). Following the theory of step-growth polymerization, the value of n_x can be used to calculate the following quantities: (1) Number-average degree M_n of polymerization

$$M_n = \frac{\sum x n_x}{\sum n_x} = \frac{1}{1 - f_{v-v}} = \frac{1}{1 - \dfrac{c_{v-v}}{c_{v0}}} \quad \text{(Eq. S11)}$$

and number fractions *P* of end-capped nanopolymers

Case of nanopolymers with active ends

$$P_{0e} = \frac{\sum n_{x,0e}}{\sum n_x} = \frac{(2c_{v0} - 2c_{v-v} - c_{v-e})^2}{(2c_{v0} - 2c_{v-v})^2} \quad \text{(Eq. S12)}$$

Case of one-end-capped prepolymers

$$P_{1e} = \frac{\sum n_{x,1e}}{\sum n_x} = \frac{2(2c_{v0} - 2c_{v-v} - c_{v-e})c_{v-e}}{(2c_{v0} - 2c_{v-v})^2} \quad \text{(Eq. S13)}$$

Case of both-end-capped prepolymers

$$P_{2e} = \frac{\sum n_{x,2e}}{\sum n_x} = \frac{c_{v-e}^{\ 2}}{(2c_{v0} - 2c_{v-v})^2} \quad \text{(Eq. S14)}$$

S2.2 Programmable coassembly of DNA-based multicomponent mixtures for star nanopolymers

In this subsection, we extend the polymerization kinetics model to predict the programmable coassembly of DNA-based multicomponent mixtures for the construction of star nanopolymers through the coupling-onto and core-first protocols. The multicomponent mixtures consist of branch-shaped motifs **Y**, bivalent DNA-NPs **v** and DNA molecules including stoppers **s** and linkers **l**. The formation of star nanopolymers is described by a series of hybridization reactions of DNA strands:

Reaction 1: for the homopolymerization of DNA-NPs **v** as shown in Eq. S5

Reaction 2: for the hybridization reaction of DNA-NPs **v** with the DNA molecules **l** and **s** as shown in Eq. S6

Reaction 3: for the dimerization of DNA molecules **l** and **s** as shown in Eq. S7

Reaction 4: for the hybridization reaction of DNA molecules **l** with the sticky ends of DNA molecules $\mathbf{y_i}$ in the motifs **Y**

$$l + y_i \underset{k_{d,l-y}}{\overset{k_{a,l-y}}{\Longleftrightarrow}} l - y_i$$

is described by the kinetic equation

$$\frac{dc_{l-y}}{dt} = k_{a,l-y}c_{l,free}c_{y,free} - k_{d,l-y}c_{l-y} = k_{a,l-y}(c_{l0} - c_{l-y})(c_{y0} - c_{l-y}) - k_{d,l-y}c_{l-y} \quad \text{(Eq. S15)}$$

where $k_{a,l\text{-}y}$ and $k_{d,l\text{-}y}$ are respectively the assembly and disassembly rate constants of DNA molecules **l** and $\mathbf{y_i}$. This additional reaction leads to the ligation between cores and arms. It should be mentioned that the branch-shaped motifs remain stable and the dehybridization events of DNA duplex can be ignored at the lower temperature. [S11,S12]

Similar to the deduction of rate constants in the Subsection S2.1, the values of k_a and k_d can be derived from fitting the variations of bond concentrations c in terms of the coassembly time (e.g., Figure S7a). For the coupling-onto and core-first protocols, the initial values for the numerical solutions of Eqs. S5-S7 and S12 are shown in Table S1.

Table S1. Initial values of numerical solutions

	Coupling-onto	Core-first
c_{v0}	$X_a C_{V0}$[a]	-[c]
c_{y0}	$3C_{Y0}$	$3C_{Y0}$
c_{l0}	C_{V0}	-
c_{s0}	C_{V0}	-
$c_{v\text{-}v}$	$(X_a\text{-}1)C_{V0}$	0

$c_{v\text{-}s}$	C_{V0}	0
$c_{v\text{-}l}$	C_{V0}	0
$c_{l\text{-}y}$	0	0
$c_{y\text{-}y}$	$3C_{Y0}$	$3C_{Y0}$
n_v	$X_a N_{V0}$[b]	-
n_y	$3N_{Y0}$	$3N_{Y0}$

[a] C_{Y0} and C_{V0} are the initial concentrations of the branch-shaped motifs **Y** and the both-end-capped prepolymers **V** containing X_a NPs, respectively.

[b] N_{Y0} and N_{V0} are the initial numbers of the branch-shaped motifs **Y** and the end-capped prepolymers **V**, respectively.

[c] '-' means that the initial concentration corresponds to the initial value of the respective component.

The concentrations c of distinct bonds can be used to deduce the number n_x of coassemblies with x NPs (Note that the uppercase letter X in Section 3 is used to represent the number of building units including NP and motifs Y)

$$n_x = n_{x,V} + n_{x,S1} + n_{x,S2} + n_{x,S3} \quad \text{(Eq. S16)}$$

where $n_{x,V}$ is the number of end-capped prepolymers, and $n_{x,Si}$ (i = 1, 2 and 3) are the numbers of i-arm star nanopolymers. The number $n_{x,V}$ of end-capped prepolymers is written as

$$n_{x,V} = n_v C_{x-1}^{0} f_{v-v}^{x-1}(1 - f_{v-v})(1 - f_{v-v} - f_{v-y}) \quad \text{(Eq. S17)}$$

where n_v is the total number of DNA-NPs and C_{x-1}^{i} is the binomial coefficient. $f_{v\text{-}v} = c_{v\text{-}v}/c_{v0}$ is the fraction of grafted DNA strands reacted with the complementary DNA strands to form the v-v bonds. The combined fraction $f_{v\text{-}y} = c_{v\text{-}l}c_{l\text{-}y}/(c_{v0}c_{l0})$ of grafted DNA strands reacted with the DNA molecules **y** includes the contributions of the connection between DNA molecules $\mathbf{y}_i$ and **l** as well as the connection between DNA molecule **l** and DNA-NPs **v**, which lead to the linkage of branch-shaped motifs **Y** and end-capped prepolymers **V**. Similarly, the number $n_{x,Si}$ (i = 1, 2 and 3) of i-arm star nanopolymers can be written as

$$n_{x,Si} = n_v C_{x-1}^{i-1} f_{v-v}^{x-i}(1 - f_{v-v})^i \frac{C_3^i}{3} f_{v-y}\left(\frac{c_{v0}}{c_{y0}} f_{v-y}\right)^{i-1}\left(1 - \frac{c_{v0}}{c_{y0}} f_{v-y}\right)^{3-i} \quad \text{(Eq. S18)}$$

The total number Σn_x of coassemblies is given by

$$\frac{\sum n_x}{n_v} = 1 - f_{v-v} - \frac{c_{v0}}{c_{y0}} f_{v-y}^{2}\left(1 - \frac{c_{v0}}{3c_{y0}} f_{v-y}\right) \quad \text{(Eq. S19)}$$

The number $n_{0,Y}$ of motifs **Y** can be written as

$$n_{0,Y} = N_{Y0}\left(1 - \frac{c_{v0}}{c_{y0}} f_{v-y}\right)^3 \quad \text{(Eq. S20)}$$

The value of n_x can be used to deduce the number-average degree M_n of polymerization

$$M_n = \frac{\sum x n_x}{\sum n_x} = \frac{1}{1 - f_{v-v} - \frac{c_{v0}}{c_{y0}} f_{v-y}^{2} \left(1 - \frac{c_{v0}}{3c_{y0}} f_{v-y}\right)}$$

(Eq. S21)

as well as the number fractions of free branch-shaped motifs **Y** and *i*-arm star copolymers $\mathbf{S_i}$

Case of free branch-shaped motifs **Y**

$$P_{Y,free} = \frac{n_{0,Y}}{N_{Y0}} = (1 - \frac{c_{v0}}{c_{y0}} f_{v-y})^3 \quad \text{(Eq. S22)}$$

Cases of *i*-arm star copolymers $\mathbf{S_i}$

$$P_{Si} = \frac{\sum n_{x,Si}}{N_{Y0}} = C_3^i \left(\frac{c_{v0}}{c_{y0}} f_{v-y}\right)^i \left(1 - \frac{c_{v0}}{c_{y0}} f_{v-y}\right)^{3-i} \quad \text{(Eq. S23)}$$

It is worth noting that the formation of miktoarm and four-arm coassemblies shown in Figure 4 of the main text share the general framework of the polymerization kinetic model for the three-arm star nanopolymers, such as the derivation of kinetic equations as well as the definition of polymerization degrees and the number fractions of coassemblies. For various architectures of star nanopolymers, the main differences lie in the initial values of kinetic equations (Table S1) and the numbers of distinct nanopolymers (Eq. S17), etc.

In consideration of the lower yield of branch-shaped motifs in the arm-first and one-step coassembly protocols (also demonstrated in Figure S5), the polymerization kinetic model cannot be applied to reliably predict the programmable coassembly of DNA-based multicomponent mixtures for the star-like coassemblies.

S2.3 Programmable coassembly of DNA-based multicomponent mixtures for graft nanocopolymers

In order to build upon the graft nanocopolymers, the sequences of sticky ends of branch-shaped motifs **Y** are designed and schematically illustrated in Figures S3 and S11. Unlike the same sequences of sticky ends for the construction of star nanopolymers, the motifs **Y** have two identical and one different sequences of sticky ends. An introduction of complementary DNA strands (i.e., the DNA linkers **l'**) triggers the hybridization of sticky ends of branch-shaped motifs **Y**, resulting in the formation of multivalent backbones. In addition to a series of hybridization reactions of DNA strands (i.e., Reactions 1-4 in Subsection S2.2), the formation of the backbones of graft nanocopolymers is also included

Table S2. Initial values of numerical solutions

	Coupling-onto	Backbone-first
c_{v0}	$X_s C_{V0}$[a]	-[c]
c_{y0}	$3C_{Y0}$	$3C_{Y0}$

c_{l0}	C_{V0}	-
$c_{l'0}$	$2(X_b+1)/X_bC_{Y0}$	$2(X_b+1)/X_bC_{Y0}$
c_{s0}	C_{V0}	-
$c_{v\text{-}v}$	$(X_s\text{-}1)C_{V0}$	0
$c_{v\text{-}s}$	C_{V0}	0
$c_{v\text{-}l}$	C_{V0}	0
$c_{l\text{-}y}$	0	0
$c_{l'\text{-}y}$	$2C_{Y0}$	$2C_{Y0}$
$c_{y\text{-}y}$	$3C_{Y0}$	$3C_{Y0}$
n_v	X_sN_{V0}[b]	-
n_y	$3N_{Y0}$	$3N_{Y0}$

[a] C_{Y0} and C_{V0} are the initial concentrations of the branch-shaped motifs **Y** and the end-capped prepolymers **V**, respectively. X_s and X_b are the lengths of graft sidechains and backbone, respectively.

[b] N_{Y0} and N_{V0} are the initial numbers of the branch-shaped motifs **Y** and the end-capped prepolymers **V**, respectively.

[c] '-' means that the initial concentration corresponds to the initial value of the respective component.

Reaction 5: for the hybridization reaction of DNA molecules **l'** with sticky ends of DNA molecules $\mathbf{y_i}$ (i = 2 and 3)

$$l' + y_i \underset{k_{d,l'-y}}{\overset{k_{a,l'-y}}{\Longleftrightarrow}} l'-y_i$$

is described by the kinetic equation

$$\frac{dc_{l'-y}}{dt} = k_{a,l'-y}c_{l',free}c_{y,free} - k_{d,l'-y}c_{l'-y} = k_{a,l'-y}\left(c_{l'0} - c_{l'-y}\right)\left(\frac{2}{3}c_{y0} - c_{l'-y}\right) - k_{d,l'-y}c_{l'-y} \quad \text{(Eq. S24)}$$

where $k_{a,l'-y}$ and $k_{d,l'-y}$ are respectively the assembly and disassembly rate constants of DNA molecules **l'** and $\mathbf{y_i}$. For the backbone-first and coupling-onto coassembly protocols, where the number of active sites of backbones is fixed, the initial values for the numerical solutions of Eqs. S5-S7, S15 and S24 are shown in Table S2.

(**Backbone**) The backbone of graft nanocopolymers is formed by x branch-shaped motifs **Y** linked by the DNA molecules **l'**, which are designated by Y~Y bonds. The graft nanocopolymers with x branch-shaped motifs **Y** have (x -1) Y~Y bonds and their number n_x^B is given by

$$n_x^B = n_{x,0e}^B + n_{x,1e}^B + n_{x,2e}^B \quad \text{(Eq. S25)}$$

where $n_{x,ie}^{B}$ is the number of backbones with *i* ends of DNA molecules **l'**. The value of n_x is written as

$$n_x^B = N_{Y0} f_{Y\sim Y}^{x-1} f_{Y,free}^{\ 2} + 2N_{Y0} f_{Y\sim Y}^{x-1} f_{Y,free} f_{l',free} + N_{Y0} f_{Y\sim Y}^{x-1} f_{l',free}^{\ 2} = N_{Y0} f_{Y\sim Y}^{x-1} (f_{Y,free} + f_{l',free})^2 \quad \text{(Eq. S26)}$$

where $f_{Y,\,free} = (2/3\ c_{y,0} - c_{l'\text{-}y})/(2/3\ c_{y,0})$ is the fraction of unreacted DNA molecules $\mathbf{y_i}$ (*i* = 2 and 3). The fraction of unreacted linkers **l'** is given by $f_{l',\,free} = f_{Y\text{-}l'}\,(f_B - f_{Y\text{-}l'})$, where $f_B = (2c_{l',0})/(2/3c_{y,0}) \geq 1$ represents the ratio of the concentration of the DNA molecule $\mathbf{y_i}$ to linkers **l'** and $f_{Y\text{-}l'} = c_{l'\text{-}y}/(2/3\ c_{y,0})$ is the hybridization probability between branch-shaped motifs **Y** and linkers **l'**. $f_{Y\sim Y} = f_{Y\text{-}l'}(1 + f_{Y\text{-}l'} - f_B)$ represents the fraction of Y~Y bonds through the hybridization between branch-shaped motifs **Y** and linkers **l'**. Number-average polymerization degree M_n of backbones **B** is written as

$$M_n = \frac{\sum x n_x^B}{\sum n_x^B} = \frac{1}{1 - f_{Y\sim Y}} \quad \text{(Eq. S27)}$$

Number fractions of backbones with various ends of DNA molecules **l'** are listed as follows

Case of backbones without the DNA molecules **l'**

$$P_{0e} = \frac{\sum n_{x,0e}^{B}}{\sum n_x^B} = \frac{f_{Y,free}^{\ 2}}{\left(f_{Y,free} + f_{l',free}\right)^2} \quad \text{(Eq. S28)}$$

Case of backbones with one end of DNA molecules **l'**

$$P_{1e} = \frac{\sum n_{x,1e}^{B}}{\sum n_x^B} = \frac{2 f_{Y,free} f_{l',free}}{\left(f_{Y,free} + f_{l',free}\right)^2} \quad \text{(Eq. S29)}$$

Case of backbones with both ends of DNA molecules **l'**

$$P_{2e} = \frac{\sum n_{x,2e}^{B}}{\sum n_x^B} = \frac{f_{l',free}^{\ 2}}{\left(f_{Y,free} + f_{l',free}\right)^2} \quad \text{(Eq. S30)}$$

(**Graft nanocopolymers**) For the backbone-first and coupling-onto coassembly protocols, where the number X_b of active sites of backbones is fixed, the number n_x of coassemblies with *x* NPs is given by

$$n_x = n_{x,V} + n_{x,G1} + n_{x,G2} + \cdots + n_{x,GX_b} \quad \text{(Eq. S31)}$$

where $n_{x,V}$ is the number of free nanopolymers and $n_{x,Gns}$ (n_s = 1, ⋯, X_b) is the number of graft nanocopolymers with n_s graft sidechains. Like Eq. S17, the number $n_{x,V}$ of free nanopolymer is written as

$$n_{x,V} = n_v C_{x-1}^{0} f_{v-v}^{x-1}(1-f_{v-v})(1-f_{v-v}-f_{v-y}) \quad \text{(Eq. S32)}$$

The formation of graft nanocopolymers includes the contributions from the y_i-l, l-v and y_i-l′ connections. Therefore, the number $n_{x,Gns}$ of graft nanocopolymers with n_s graft sidechains can be written as

$$n_{x,Gns} = C_{x-1}^{n_s-1} n_v f_{v-v}^{x-n_s}(1-f_{v-v})^{n_s}\frac{C_{Y0}}{c_{v0}} f_{Y\sim Y}^{X_b-1}(1-f_{Y\sim Y})^2 C_{X_b}^{n_s}\left(\frac{c_{v0}f_{v-y}}{c_{Y0}}\right)^{n_s}\left(1-\frac{c_{v0}f_{v-y}}{c_{Y0}}\right)^{X_b-n_s} \quad \text{(Eq. S33)}$$

The total number Σn_x of coassemblies is given by

$$\frac{\sum n_x}{n_v} = 1-f_{v-v}-f_{v-y}+\frac{f_{v-y}(1-f_{Y\sim Y})}{1-f_{Y\sim Y}(1-c_{v0}f_{v-y}/c_{Y0})} \quad \text{(Eq. S34)}$$

The number $n_{0,B}$ of backbones can be written as

$$n_{0,B} = N_{Y0}(1-f_{Y\sim Y})\left(1-\frac{c_{v0}f_{v-y}}{c_{Y0}}\right)^{X_b} \quad \text{(Eq. S35)}$$

Thus, one can deduce the number-average polymerization degree M_n of coassemblies given by

$$M_n = \frac{\sum x n_x}{\sum n_x} = \frac{1}{1-f_{v-v}-f_{v-y}+f_{v-y}(1-f_{Y\sim Y})/(1-f_{Y\sim Y}(1-c_{v0}f_{v-y}/c_{Y0}))} \quad \text{(Eq. S36)}$$

The number fractions of backbone and graft polymers are listed as follows

Case of backbones **B**

$$P_B = \frac{\sum_{X_b=1}^{\infty} n_{0,B}}{\sum n_x^B} = \frac{N_{Y0}(1-f_{Y\sim Y})\left(1-\frac{c_{v0}f_{v-y}}{c_{Y0}}\right)^{X_b}}{N_{Y0}(1-f_{Y\sim Y})} = \left(1-\frac{c_{v0}f_{v-y}}{c_{Y0}}\right)^{X_b} \quad \text{(Eq. S37)}$$

Case of graft nanocopolymers $\mathbf{G_{ns}}$ (n_s = 1, ⋯, X_b) with n_s sidechains

$$P_{Gns} = \frac{\sum_{x=n_s}^{\infty} n_{x,Gns}}{\sum n_x^B} = C_{X_b}^{n_s}\left(\frac{c_{v0}f_{v-y}}{c_{Y0}}\right)^{n_s}\left(1-\frac{c_{v0}f_{v-y}}{c_{Y0}}\right)^{X_b-n_s}$$

(Eq. S38)

It is worthy of pointing out that the reduced temperature of system plays a crucial role in tailoring the programmable coassembly of DNA-based multicomponent mixtures. [S13,S14] In the generalized polymerization kinetics model proposed herein, the coassembly of DNA-based multicomponent mixtures can be described by a family of hybridization/dehybridization events of complementary DNA strands, determining by their rate constants in the elementary reactions. As evidenced in Figure S8, the rate constants can be tailored by the change of reduced temperature. This observation implies that generalized polymerization kinetics model have the capability to capture the temperature-dependent coassembly behaviors of DNA-based multicomponent mixtures.

S3. Scaling relationship of branch-shaped coassemblies

We first characterize the dimension of branch-shaped coassemblies of DNA-based multicomponent mixtures. The best quantity to characterize the overall dimension of branch-shaped coassemblies is the mean-squared radius $\langle R_g^2 \rangle$ of gyration. Similar to the definition of molecular polymers, [S15, S16] the mean-squared gyration radius $\langle R_g^2 \rangle$ of branch-shaped co-assemblies containing *X* building units is given by

$$\langle R_g^2 \rangle \equiv \left\langle \sum_{i,j=1}^{X} (R_i - R_j)^2 \right\rangle / 2X^2 \quad \text{(Eq. S39)}$$

where $\mathbf{R}_{i(j)}$ is the center coordinates of *i*(*j*)-th building units (i.e., nanoparticles **v** and motifs **Y**).

An important aspect about the dimension of coassemblies with branching nanoarchitectures is the change with respect to the polymerization degree *X* (i.e., the scaling relationship). Typically, for the star nanoarchitecture, the scaling relationship is expressed in the following form [S17-S18]

$$\langle R_g^2 \rangle_{star}^{1/2} \sim X_a^{0.6} n_a^{0.2} \quad \text{(Eq. S40)}$$

where X_a and n_a are respectively the length and number of arms. For the graft nanoarchitecture, the scaling relationship of coassemblies is more complex. Using the Flory's mean-field argument, it is shown that the radius of gyration should scale according to the following formula [S19-S20]

$$\langle R_g^2 \rangle_{graft}^{1/2} \sim \left(1 + X_s \times \frac{n_s}{X_b}\right)^{0.4} X_b^{0.6} \cong X_s^{0.4} n_s^{0.4} X_b^{0.2} \quad \text{(Eq. S41)}$$

where X_b is the length of backbones, and X_s and n_s are respectively the length and number of graft sidechains.

Another important aspect about the dimension of branch-shaped coassemblies is the branching index that is widely used to describe the degree of branching in the polymer science. [S21] The branching index compares the mean-squared dimension of nonlinear nanopolymers to linear nanopolymers that consist of the same number of building units. For the mean-squared radius of gyration, the branching index *g*' is defined as [S22-S23]

$$g' = \frac{\langle R_g^2 \rangle}{\langle R_g^2 \rangle_l} \quad \text{(Eq. S42)}$$

where $\langle R_g^2 \rangle_l$ is the mean-squared gyration radius of linear coassemblies with the same number of building units. For the regular star nanoarchitecture, the branching index *g*' from the prediction of the Zimm-Stockmayer equation is calculated as [S29]

$$g' = \frac{(3n_a - 2)}{n_a^2} \quad \text{(Eq. S43)}$$

For the graft nanoarchitecture, the predicted branching index *g*' is given by

$$g' = \frac{(X_b^3 + 2n_s X_b^2 X_s + n_s(n_s + 2)X_b X_s^2 + (3n_s^2 - 2n_s)X_s^3)}{(X_b + X_s n_s)^3}$$

(Eq. S44)

S4. Additional figures for construction of star nanopolymers

S4.1 Construction of branch-shaped motifs

The programmable self-assembly of DNA molecules $\mathbf{y_1}$, $\mathbf{y_2}$ and $\mathbf{y_3}$ is used to construct the branch-shaped motifs **Y**, which are schematically illustrated in Figure 2a of the main text. The sequences of DNA molecules $\mathbf{y_1}$, $\mathbf{y_2}$ and $\mathbf{y_3}$ are listed in Figure S2. In the quenched simulations, the initial states are the random configurations of DNA molecules $\mathbf{y_1}$, $\mathbf{y_2}$ and $\mathbf{y_3}$ and the reduced temperature is set as $T^* = 0.95$. Usually, the DNA molecules quickly self-assemble into the branch-shaped motifs **Y** (highlighted by red in Figure S5a) driven by the hybridization of complementary sequences of DNA molecules $\mathbf{y_1}$, $\mathbf{y_2}$ and $\mathbf{y_3}$. However, the resulting configuration of quenched simulations contains lots of mismatched nanostructures of DNA assemblies, which are represented by gray color in Figure S5a and schematically drawing in Figure S5b. The yield of the branch-shaped motifs **Y** is extremely low (e.g., 10%) in the quenched simulations.

To boost the yield of branch-shaped motifs **Y**, a multiple annealing process is proposed in the coarse-grained simulations and schematically illustrated in Figure S5c. Specifically, multiple annealing events (their number designated as n_A) occur in the course of the programmable self-assembly of DNA molecules from the initial temperature ($T^*_i > T_m$ of melt temperature) to the end temperature ($T^*_e = 0.95$). In the *i*-th annealing event, the *i*-th initial and end temperatures are respectively set as $T^*_{i,i} = T^*_i - (i\text{-}1)\times\Delta$ and $T^*_{i,e} = T^*_i - i\times\Delta$ under $\Delta = (T^*_i - T^*_e)/n_A$. The reduced temperature T^* linearly increases to $T^*_{i,i} + \Delta/2$ with the simulation step and then quadratically decreases to $T^*_{i,e}$. The above procedure is repeated n_A times until the reduced temperature T^* approaches the end temperature T^*_e. The total time step of annealing simulations is 2.5×10^9. When the yield of branch-shaped motifs remains within a narrow fluctuation around a constant value in spite of an extension of additional time step of 1.0×10^6, the annealing simulations of programmable self-assembly of DNA molecules are regarded as the achievement of equilibrium states. It is found that the number n_A of annealing events plays an important role in affecting the yield of branch-shaped motifs **Y** (Figure S5d). Namely, an increase in the number of annealing events can facilitate the formation of branch-shaped motifs **Y** and the yield can achieve ~80% under the condition of $n_A = 3$ or 5. However, when the number of annealing events is further increased, no significant improvement in yield is observed. The findings confirm the fact that five annealing events are sufficient for the reliable formation of branch-shaped motifs **Y**.

It should be mentioned that the annealing process is specifically applied for the construction of branch-shaped motifs during the programmable self-assembly of DNA molecules, and isn't applied for the subsequent coassembly of DNA-based multicomponent mixtures. Especially, in both the coupling-onto and core-first protocols, the mismatched nanostructures of DNA assemblies are excluded in subsequent coarse-grained simulations of coassembly. Given the high yield of well-defined branch-shaped motifs, the presence of such impurities has a negligible impact on both the formation kinetics and the overall production of star nanopolymers in these protocols.

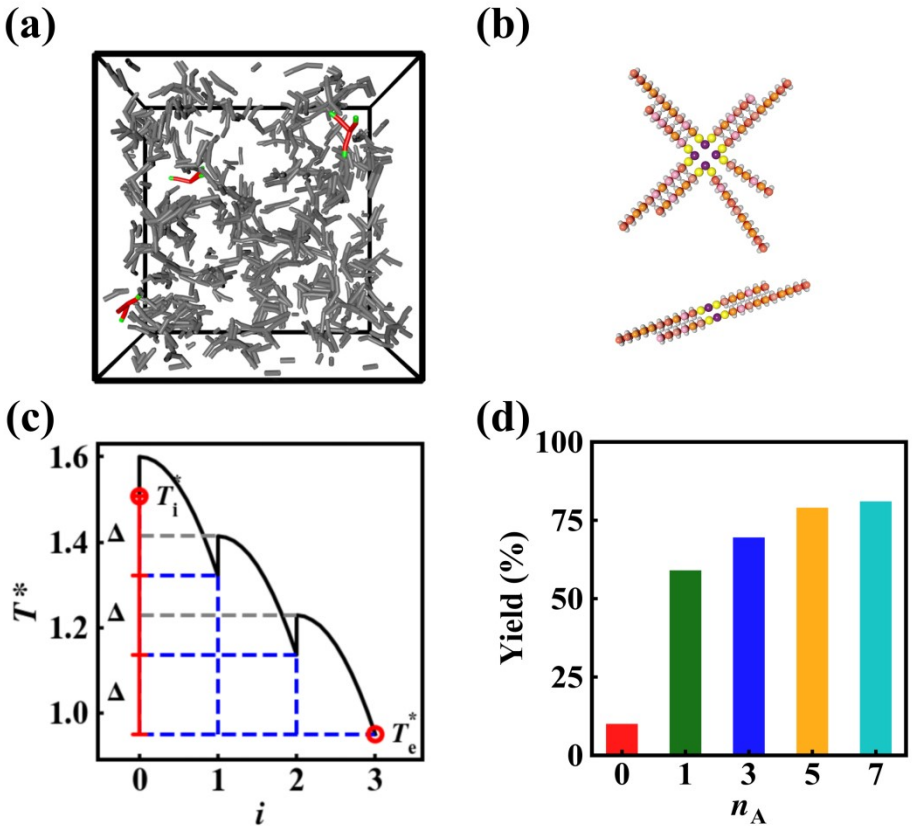

Fig. S5: (a) Self-assembled nanostructures of DNA molecules $\mathbf{y_1}$, $\mathbf{y_2}$ *and* $\mathbf{y_3}$ *quenching to the reduced temperature* $T^* = 0.95$. *The stems and sticky ends of branch-shaped motifs* **Y** *are highlighted in red and green colors, respectively. (b) Mismatched nanostructures of DNA assemblies. These nanostructures and free DNA molecules in the quenched simulations are indicated by the gray color in panel (a). (c) Reduced temperature* T^* *in terms of the i-th annealing event. (d) Yield of branch-shaped motifs* **Y** *in terms of the number* n_A *of annealing events.* $n_A = 0$ *corresponds to the case of quenched simulations.*

S4.2 Prepolymerization of DNA-NPs

Monovalent DNA molecules **s** as stoppers and **l** as linkers (both designated as **e** in this subsection) are introduced into the polymerization of DNA-NPs **v** for the achievement of both-end-capped prepolymers **V**, which are schematically illustrated in Figure 2b of the main text. The sequences of grafted and monovalent DNA molecules are depicted in Figure S2. Figure S6a shows the variation in the concentrations c of v-v, v-e and e-e bonds as well as free DNA-NPs **v** and DNA molecules **e**. The NPs **v** are dressed by DNA strands with complementary sequences, whose hybridization triggers the formation of v-v bonds. In contrast, the DNA molecules **e** stop the polymerization of DNA-NPs **v** due to the existence of an inhibiting sequence of linkers **l** or the exhausted sequence of stoppers **s**, resulting in the formation of v-e bonds. The e-e bonds arise from the hybridization of complementary sequences of DNA molecules **l** and **s**. In general, the free DNA-NPs and DNA molecules are quickly consumed at the initial stage of simulations due to the formation of v-v and v-e bonds, and the v-v bonds connecting the DNA-NPs reach a plateau at later stage.

The assembly kinetics and production of prepolymers can be tuned by the initial ingredient f of the prepolymerization system, which is defined as the ratio of the concentration of monovalent DNA molecules to that of DNA-NPs. The growth of DNA-NP chains is characterized by a temporal change in the number-average degree M_n of polymerization as $M_n = \sum n_x x / \sum n_x$, where x is the number of NPs in assemblies and n_x is the number of assemblies containing x NPs. If monovalent DNA molecules bind to linear chains of DNA-NPs, they add 'dead' ends to the chains, and the polymerization of bivalent DNA-NPs is suppressed or completely stopped. Therefore, the presence of monovalent DNA molecules **l** and **s** as chain stoppers remarkably decreases the average chain length M_n of prepolymers (Figure S6b). In particular, as shown in Figure S6c, the prepolymerization system at the initial ingredient f = 0.50 has the capability to predominantly assemble into the prepolymers containing ~5 NPs, which are capped with DNA molecules at both ends (i.e., both-end-capped prepolymers).

By fitting numerical solutions of kinetic equations in Eqs. S5-S7 to the simulation data of intermonomer bonds presented in Figure S6a, we can derive the assembly and disassembly rate constants $k_{a/d,\,\alpha}$ (α = v-v, v-e and e-e bonds), which are depicted in Figure S6d. These assembly and disassembly rate constants can be used to predict the number-average degree M_n of polymerization and the number fractions P of prepolymers on the basis of the theoretical model in Subsection S2.1. As can be seen, the data points obtained from the coarse-grained simulations are in excellent agreement with the predictions of the theoretical model, which are represented by solid lines in Figure S6b and c.

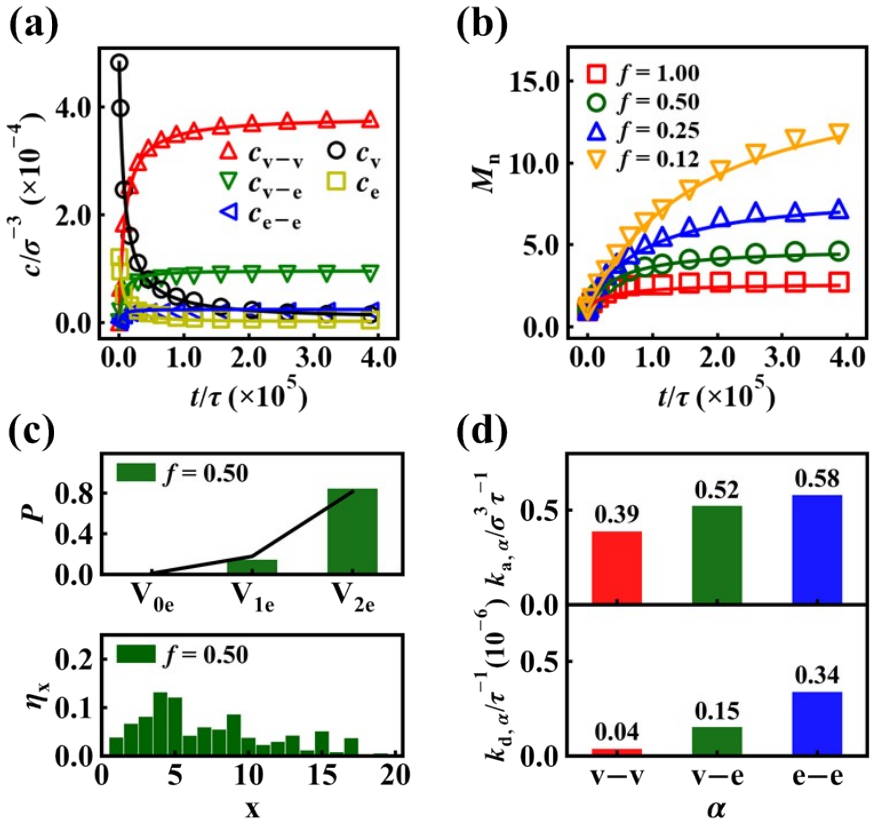

*Fig. S6: (a) Variation in the concentrations c of v-v, v-e and e-e bonds as well as free DNA-NPs and DNA molecules. The solid lines represent the best fit for Eqs. S5-S7. (b) Temporal evolution of number-average degree M_n of polymerization under various initial ingredients f. (c) Number fraction P of nanopolymers with active ends (**V_{0e}**), one-end-capped prepolymers (**V_{1e}**) and both-end-capped prepolymers (**V_{2e}**) and weight fraction η_x of nanopolymers with the polymerization degree x at assembly time $t = 4.0\times10^5\tau$ and initial ingredient $f = 0.50$. In panels (b) and (c), the solid lines are the predicted values of the theoretical model. (d) Assembly and disassembly rate constants $k_{a,\alpha}$ and $k_{d,\alpha}$ (α = v-v, v-e and e-e bonds). The case of α = v-e corresponds to the rate constants $k_{a/d,v\text{-}s}$ and $k_{a/d,v\text{-}l}$. The case of α = e-e corresponds to the rate constants $k_{a/d,l\text{-}s}$. The error bars are not shown for clarity.*

S4.3 Star nanopolymers through coupling-onto protocol

Figure S7 shows the coassembly kinetics of branch-shaped motifs **Y** and end-capped prepolymers **V** for the construction of star nanopolymers through the coupling-onto protocol. As shown in Figure S7a, the y-y, v-l and v-v bonds are preserved in the course of coassembly, but the concentration of l-y bond has a remarkable increase, further demonstrating the formation of star nanopolymers due to the linkages of the formed motifs **Y** and prepolymers **V**. In particular, the fraction of free prepolymers **V** shows a notable decrease in the early stage, while the fractions of star nanopolymers $\mathbf{S_1}$ and $\mathbf{S_2}$ with one and two arms increase rapidly and reach a peak (Figure S7b). Subsequently, the fractions of star nanopolymers $\mathbf{S_1}$ and $\mathbf{S_2}$ show a decrease, but the fraction of three-arm star nanopolymers $\mathbf{S_3}$ increases, suggesting that the formation of three-arm star nanopolymers originates from the coupling between coassemblies $\mathbf{S_2}$ and free prepolymers **V**.

The assembly and disassembly rate constants $k_{a/d,\ l\text{-}y}$ can be also obtained by fitting numerical solutions of kinetic equations to the simulation data of intermonomer bonds presented in Figure S7a. Figure S7c shows the rate constants $k_{a,\ l\text{-}y}$ and $k_{d,\ l\text{-}y}$ in terms of the initial ingredient F_s of coassembly system. It can be found that the rate constants are weakly dependent upon the initial ingredient F_s. The assembly and disassembly rate constants for the linkage of branch-shaped motifs **Y** and end-capped prepolymers **V** have values of $k_{a,\ l\text{-}y} = 0.39\ \sigma^3\tau^{-1}$ and $k_{d,\ l\text{-}y} = 3.0\times10^{-8}\tau^{-1}$, respectively.

Figure S8 shows the effect of reduced temperature T^* on the coassembly of motifs **Y** and prepolymers **V** for the construction of star nanopolymers. As shown in Figure S8a, the assembly rate constants $k_{a,\ \alpha}$ (α = v-v, v-e and l-y bonds) decrease with an increase in the reduced temperature, while the disassembly rate constants $k_{d,\ \alpha}$ increase, implying that the dehybridization of DNA duplexes occurs remarkably at higher temperature. As a result, the mixture of motifs **Y** and prepolymers **V** at higher temperature is programmed to coassemble into star nanopolymers with lower polymerization degree and number of arms (Figure S8b and c). It should be mentioned that the simulation data of coassembly system are well fitted by the theoretical model established in Subsection S2.2, in spite of the case of higher temperature.

Figure S9 shows the effect of initial concentration c_V of prepolymers **V** on the construction of star nanopolymers via the coupling-onto protocol. Higher initial concentration accelerates the growth of star nanopolymers and results in a larger value of polymerization degree at given time (Figure S9a). When more prepolymers **V** are added into the simulation boxes, the probability of effective collision for the connection between motifs **Y** and prepolymers **V** is largely increased. Consequently, as the initial concentration is increased, the binary mixture of end-capped prepolymers and branch-shaped motifs is programmed to coassemble into the three-arm star nanopolymers $\mathbf{S_3}$ with higher yield (Figure S9b).

Figure S10 shows the effect of chain length X_a of arms **V** on the construction of star nanopolymers. As can be seen, the chain length of arms mainly impacts the coassembly kinetics of binary mixture at the late stage (Figure S10a). In addition, an introduction of arms with various chain lengths into the binary mixture provides the possibility to tune the yield of coassembled productions. For instance, the arms with chain length $X_a = 3$, 5 and 8 respectively produce the star nanopolymers $\mathbf{S_3}$ with yields of 80%, 73% and 70% (Figure S10b).

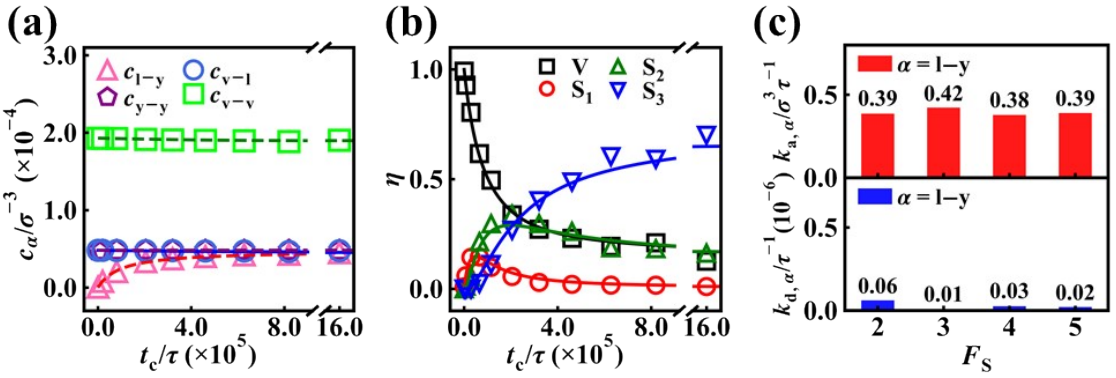

Fig. S7: (a) Variation in the concentration c of l-y, y-y, v-l and v-v bonds. (b) Weight fraction η of free prepolymers **V**, *star nanopolymers* $\mathbf{S_1}$, $\mathbf{S_2}$ *and* $\mathbf{S_3}$ *in terms of the coassembly time* t_c. *The initial ingredient is set as* $F_s = 3.0$. *(c) Assembly and disassembly rate constants* $k_{a,\ l\text{-}y}$ *and* $k_{d,\ l\text{-}y}$ *in terms of the initial ingredient* F_s. *The reduced temperature is set as* $T^* = 0.95$.

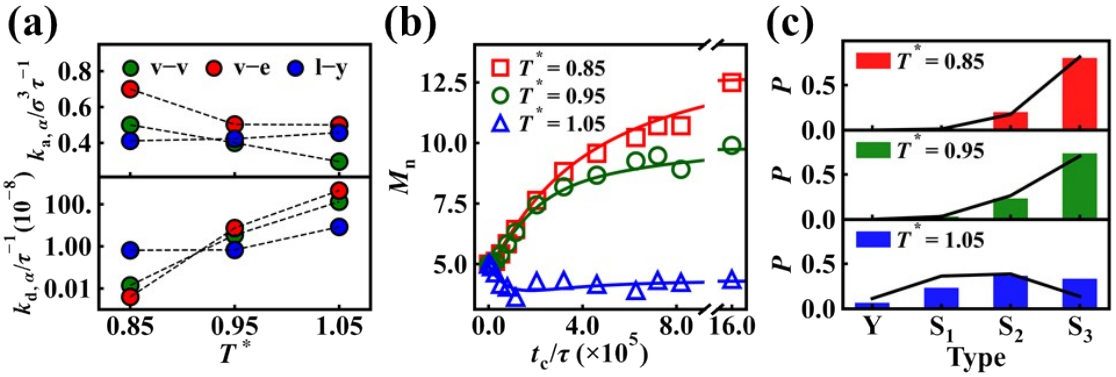

Fig. S8: Effect of reduced temperature T^* *on the construction of star nanopolymers via the coupling-onto protocol. (a) Assembly and disassembly rate constants* $k_{a,\ \alpha}$ *and* $k_{d,\ \alpha}$ *(α = v-v, v-e and l-y bond) in terms of the reduced temperature* T^*. *(b) Number-average degree* M_n *of polymerization in terms of the coassembly time* t_c. *(c) Number fraction P of free branch-shaped motifs* **Y** *and star nanopolymers* $\mathbf{S_1}$, $\mathbf{S_2}$ *and* $\mathbf{S_3}$. *The solid lines correspond to the numerical solutions of the theoretical model. The initial ingredient is set as* $F_s = 3.0$.

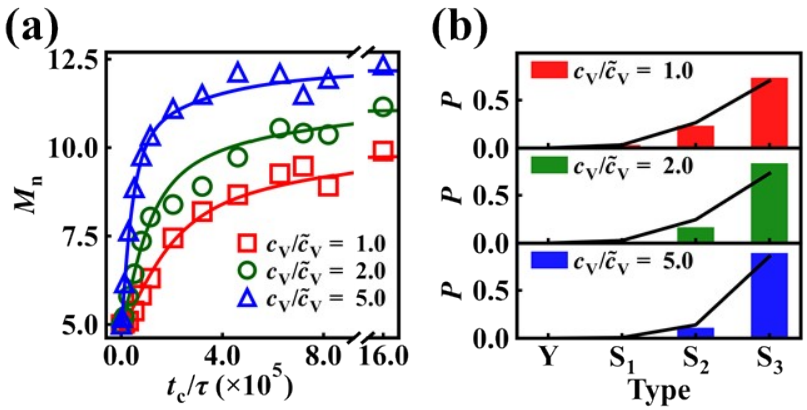

Fig. S9: Effect of initial concentration c_V of prepolymers **V** *on the construction of star nanopolymers via the coupling-onto protocol. (a) Number-average degree M_n of polymerization in terms of the coassembly time t_c. (b) Number fraction P of free branch-shaped motifs* **Y** *and star nanopolymers* **S$_1$**, **S$_2$** *and* **S$_3$**. *The initial ingredient and reduced temperature are set as F_s = 3.0 and T^* = 0.95, respectively. The reference concentration of prepolymers is given by* $\tilde{c}_V = 2.4 \times 10^{-5}\sigma^{-3}$.

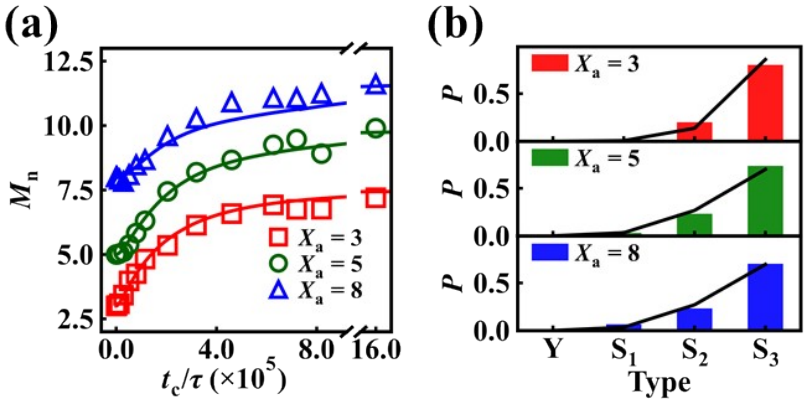

Fig. S10: Effect of chain length X_a of arms **V** *on the construction of star nanopolymers via the coupling-onto protocol. (a) Number-average degree M_n of polymerization in terms of the coassembly time t_c. (b) Number fraction P of free branch-shaped motifs* **Y** *and star nanopolymers* **S$_1$**, **S$_2$** *and* **S$_3$**. *The initial ingredient and reduced temperature are set as F_s = 3.0 and T^* = 0.95, respectively.*

S4.4 Comparison with one-pot protocol

Herein, we present the computational results of one-pot protocol as well as the comparisons with the results of coupling-onto protocol, which are shown in Figures S11. In the case of one-pot coassembly protocol, the coarse-grained simulations start from the randomly initial configurations of multicomponent mixture consisting of DNA molecules $\mathbf{y_i}$, bivalent DNA-NPs **v**, linkers **l** and stoppers **s**, which is schematically illustrated in Figure S11a. The formation of star nanopolymers is a multistep and complex process involving core formation, arm growth as well as the termination and linkage steps. The coassembly of DNA-based multicomponent mixture is a chaotic process, where all the hybridization reactions of DNA strands concurrently take place and several of kinetically trapped intermediates are identified. As a result, it is extremely difficult to achieve star nanopolymers with well-defined architecture and controllable polymerization degree (Figure S11c-f).

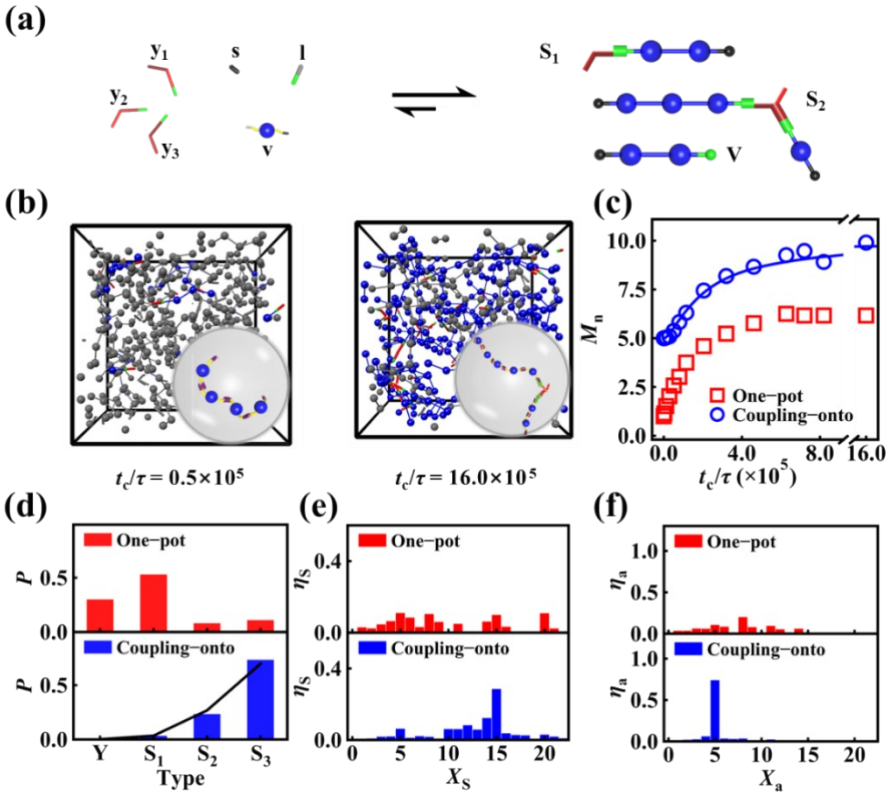

Fig. S11: Star nanopolymers constructed from one-pot protocol. (a) Schematic drawing of the coassembly of DNA-based multicomponent mixture including DNA molecules $\mathbf{y_i}$*, bivalent DNA-NPs* **v***, linkers* **l** *and stoppers* **s***. (b) Snapshots of coassembled nanostructures of DNA-based multicomponent mixture. The branch-shaped motifs* **Y** *and DNA-NPs* **v** *in the star nanopolymers are highlighted by red and blue colors, respectively. The other building units are represented by gray color. (c) Temporal evolution of number-average degree* M_n *of polymerization in the one-step and coupling-onto protocols. (d) Number fraction P of free motifs* **Y** *and star nanopolymers* $\mathbf{S_1}$, $\mathbf{S_2}$ *and* $\mathbf{S_3}$ *at the coassembly time* $t_c = 16.0\times10^5\tau$*. (e) Number fraction* η_S *of star nanopolymers as a function of their polymerization degree* X_s*. (f) Number fraction* η_a *of arms as a function of the length* X_a *of arms. The reduced temperature is set as* $T^* = 0.95$*. The solid lines represent the theoretical prediction, while the discrete symbols (dots for scatter plots and bars for bar charts) indicate the simulation data.*

S5. Additional figures for construction of graft nanocopolymers

S5.1 Graft nanocopolymers and coassembly protocols

As shown in Figure S12a, graft nanocopolymers considered in the current work are composed of a backbone **B** with several graft sidechains **V**. The backbone is constructed from the assembly of branch-shaped motifs **Y** and linkers **l'**. The sequences of DNA strands are listed in Figure S3. The design of graft sidechains is the same as the end-capped prepolymers in the star nanopolymers.

The strategies to construct the graft nanocopolymers can be categorized into three protocols: sidechain-first, backbone-first and coupling-onto protocols, which are schematically illustrated in Figure S12b-d. In the sidechain-first protocol, graft nanocopolymers are constructed from the homopolymerization of sidechains, which have polymerizable groups on the terminal of end-capped prepolymers. In the backbone-first protocol, starting from the active sites of backbones, the bivalent DNA-NPs polymerize into the sidechains of graft nanocopolymers in the presence of DNA linkers. In the coupling-onto protocol, the backbone and sidechains are independently constructed from the programmable self-assembly of branch-shaped motifs and DNA-NPs in the presence of stopper and linkers, and the coassembly of formed backbones and sidechains are used to yield the graft nanocopolymers by the coupling reaction of their active sites.

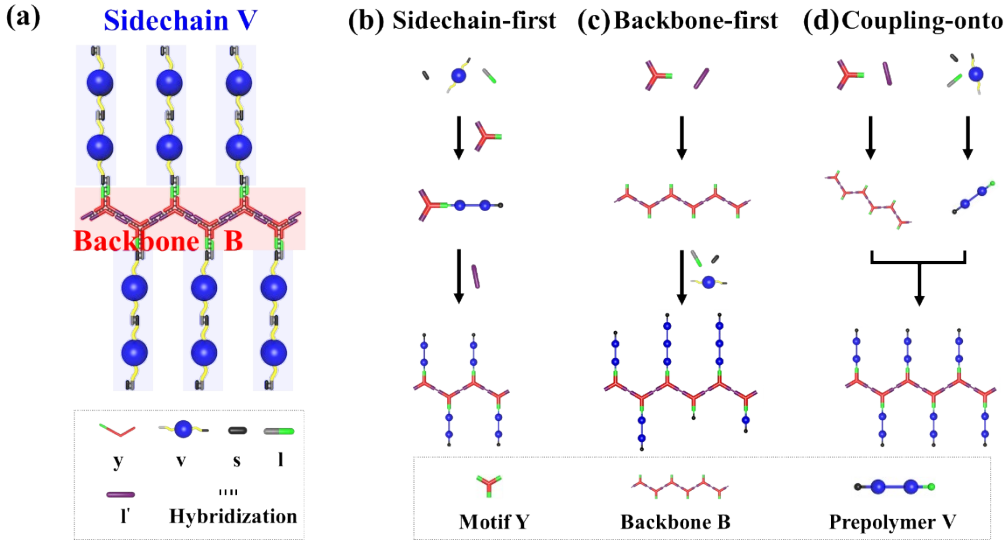

Fig. S12: (a) Illustration of graft nanocopolymers with backbone **B** *attached by end-capped prepolymers* **V** *as sidechains. (b-d) Schematic drawings of the construction protocols of graft nanocopolymers by hierarchically programmable coassembly of DNA-based multicomponent mixtures. (b) Sidechain-first, (c) backbone-first and (d) coupling-onto protocols.*

S5.2 Construction of backbones

The backbones with precise and exact placement of active sites are generated from the assembly of branch-shaped motifs **Y** and linkers **l'**. As shown in Figure S13, the assembly kinetics and mechanism are extremely similar with the prepolymerization of DNA-NPs presented in Subsection 4.2. Specifically, the initial ingredient *f'*, defined as the ratio of the concentration of linkers **l'** to that of branch-shaped motifs **Y**, plays an important role in tuning the length of backbone chains. An excess of the linkers **l'** (i.e., larger *f'*) can lead to the lower polymerization degree of backbones capped with the linkers **l'** at both ends. Furthermore, the data points obtained from the coarse-grained simulations of the assembly of branch-shaped motifs **Y** and linkers **l'** are in excellent agreement with the theoretical predictions of the prepolymerization kinetics model, which are represented by solid lines in Figure S13.

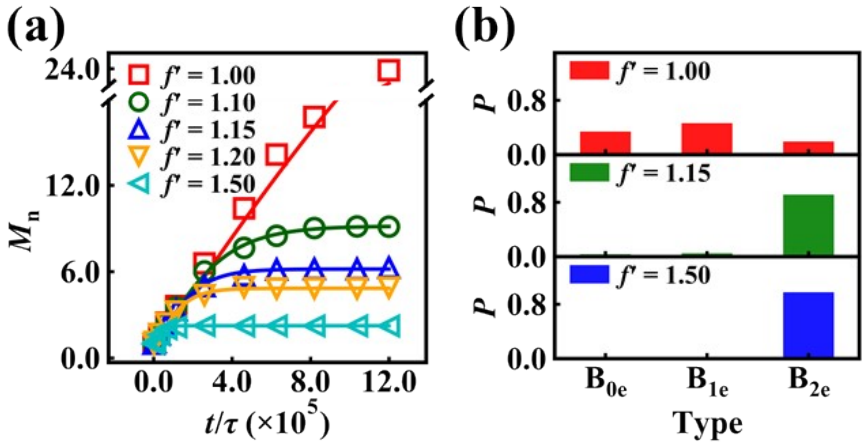

Fig. S13: Assembly of branch-shaped motifs **Y** *and linkers* **l'**. *(a) Effect of initial ingredients f' on the temporal evolution of polymerization degree* M_n *of backbones. (b) Number fraction P of backbones with active ends (*$\mathbf{B_{0e}}$*), one-end-capped backbones (*$\mathbf{B_{1e}}$*) and both-end-capped backbones (*$\mathbf{B_{2e}}$*).*

S5.3 Graft nanocopolymers through coupling-onto protocol

Figure S14 shows the coassembly kinetics of backbone **B** and sidechains **V**. By fitting numerical solutions of kinetic equations in Eqs. S5-S7, S16 and S24 to the simulation data of intermonomer bonds presented in Figure S14a, we can derive the additional assembly and disassembly rate constants $k_{a/d,\ l\text{-}y'}$, which are plotted in Figure S14b. These assembly and disassembly rate constants can be used to predict the number-average degree M_n of polymerization and the number fraction P of coassemblies on the basis of the theoretical model in Subsection S2.3.

The coassembly of binary mixture for the graft nanocopolymers can be affected by the initial concentration and the length of sidechains, which are respectively shown in Figures S15 and S16. Higher initial concentration accelerates the growth of graft nanocopolymers and results in a larger value of polymerization degree of coassemblies at a given time as well as a higher yield of graft nanocopolymers with fully grafted architectures (Figure S15). The prepolymers with the length X_s = 2, 5 and 8 of sidechains produce the fully grafted nanocopolymers with yields of 83%, 64% and 57%, respectively (Figure S16).

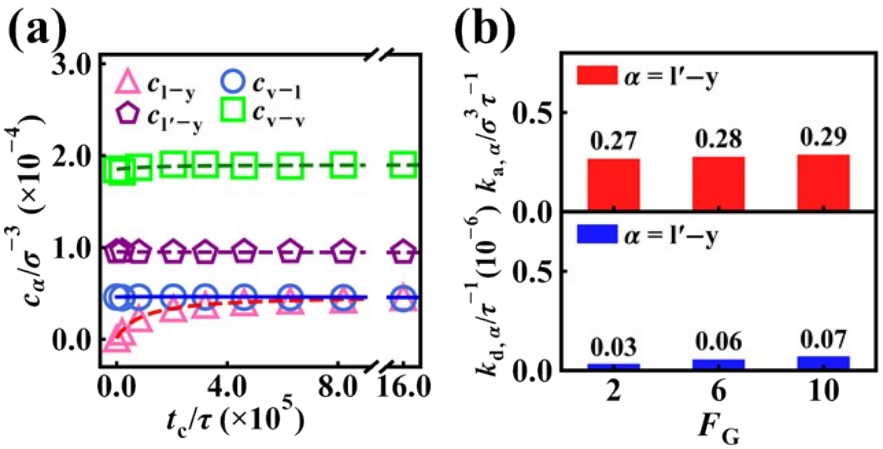

Fig. S14: (a) Variation in the concentration c of l-y, l'-y, v-l and v-v bonds. (b) Assembly and disassembly rate constants $k_{a,\ l'\text{-}y}$ and $k_{d,\ l'\text{-}y}$ in terms of the initial ingredient F_G. The reduced temperature is set as $T^* = 0.95$.

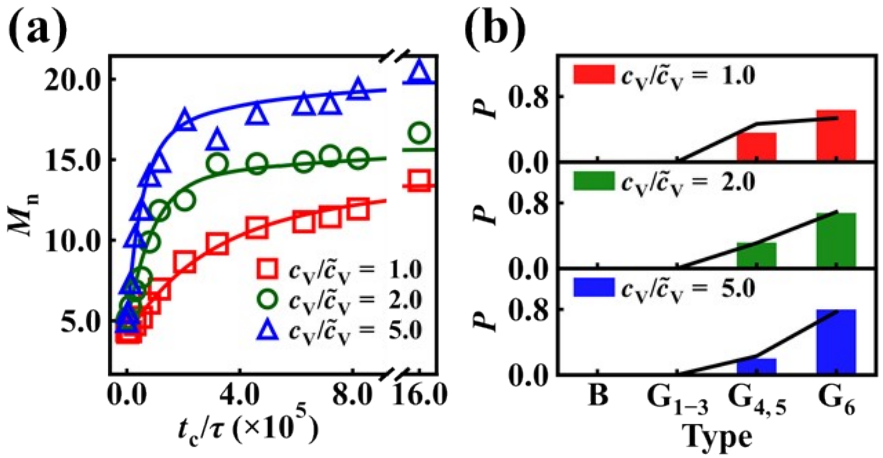

Fig. S15: Effect of initial concentration c_V of prepolymers **V** *on the construction of graft nanocopolymers. (a) Number-average degree M_n of polymerization in terms of the coassembly*

time t_c. (b) Number fraction P of free backbones **B** *and graft nanocopolymers* $\mathbf{G_{1\text{-}3}}$, $\mathbf{G_{4,5}}$ *and* $\mathbf{G_6}$. *The subscript denotes the number of sidechains. The solid lines correspond to the numerical solutions of the theoretical model. The reference concentration of prepolymers is given by* $\tilde{c}_V = 2.4 \times 10^{-5}\sigma^{-3}$.

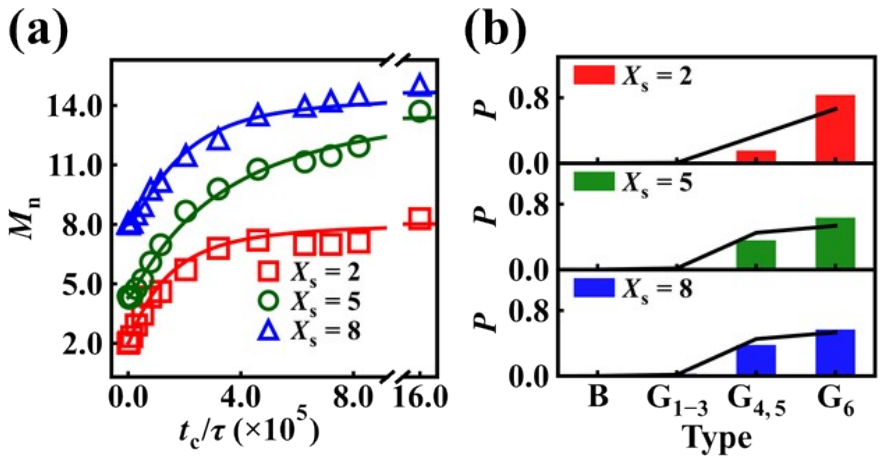

Fig. S16: Effect of length X_s of graft sidechains on the construction of graft nanocopolymers. (a) Number-average degree M_n of polymerization in terms of the coassembly time t_c. (b) Distribution P of free backbones **B** *and graft nanocopolymers* $\mathbf{G_{1\text{-}3}}$, $\mathbf{G_{4,5}}$ *and* $\mathbf{G_6}$.

S5.4 Comparison of various coassembly protocols

The graft nanocopolymers can also be constructed by the sidechain-first and backbone-first coassembly protocols of DNA-based multicomponent mixtures (Figure S12). Figures S17 and S18 respectively present the computational results of sidechain-first and backbone-first coassembly protocols as well as the comparisons with the results of coupling-onto protocol. Following the sidechain-first protocol, sidechains with polymerizable terminals are first obtained through the coupling between prepolymers **V** and branch-shaped motifs **Y** by the linkers **I**, and then the polymerizable terminals are polymerized into the graft nanocopolymers (Figure S17). The graft nanocopolymers with controllable polymerization degree and higher grafting density are achieved in the sidechain-first protocol (Figure S17c, d and f). However, the high steric hindrance in the polymerization of backbones leads to the slow polymerization kinetics and the broad distribution of coassemblies (Figure S17e).

Following the backbone-first protocol, the backbones with precise and exact placement of active sites are first generated from the polymerization of branch-shaped motifs in the presence of DNA linkers. At the active sites of backbones, bivalent DNA-NPs polymerize into the sidechains of graft nanocopolymers (Figure S18). Similar to the core-first coassembly protocol for the construction of star nanopolymers (Figure 3 of main text), the backbone-first coassembly protocol may lead to a termination of sidechain growth, resulting in the graft nanocopolymers with dead sites of backbones. This phenomenon manifests the observations of lower yield of fully branched coassemblies (Figure S18d), broad distributions of polymerization degree of coassemblies (Figure S18e) and length of graft sidechains (Figure S18f).

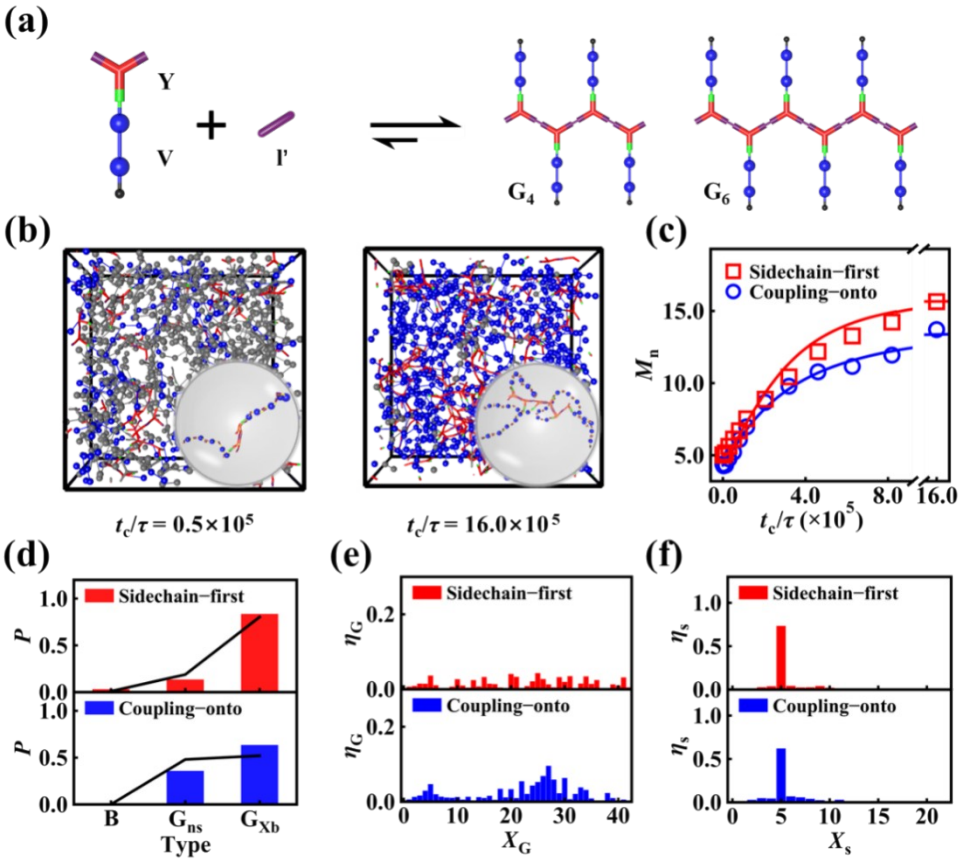

Fig. S17: Graft nanocopolymers constructed from sidechain-first protocol. (a) Schematic drawing of the construction of graft nanocopolymers. By virtue of incorporating branch-shaped motifs **Y** *into prepolymers* **V**, *the linkers* **l'** *are used to yield graft nanocopolymers with various numbers of graft sidechains. (b) Snapshots of coassembled nanostructures. The free prepolymers are represented by the gray color. (c) Temporal evolution of number-average degree M_n of polymerization under the sidechain-first and coupling-onto protocols. (d) Number fraction P of free backbones* **B** *and graft nanocopolymers* $\mathbf{G_{ns}}$ *with various numbers n_s of graft sidechains. Note that* $\mathbf{G_{Xb}}$ *represents the fully grafted nanopolymers. (e) Number fraction η_G of graft nanocopolymers as a function of their polymerization degree X_G. (f) Number fraction η_s of graft sidechains as a function of the length X_s of sidechains.*

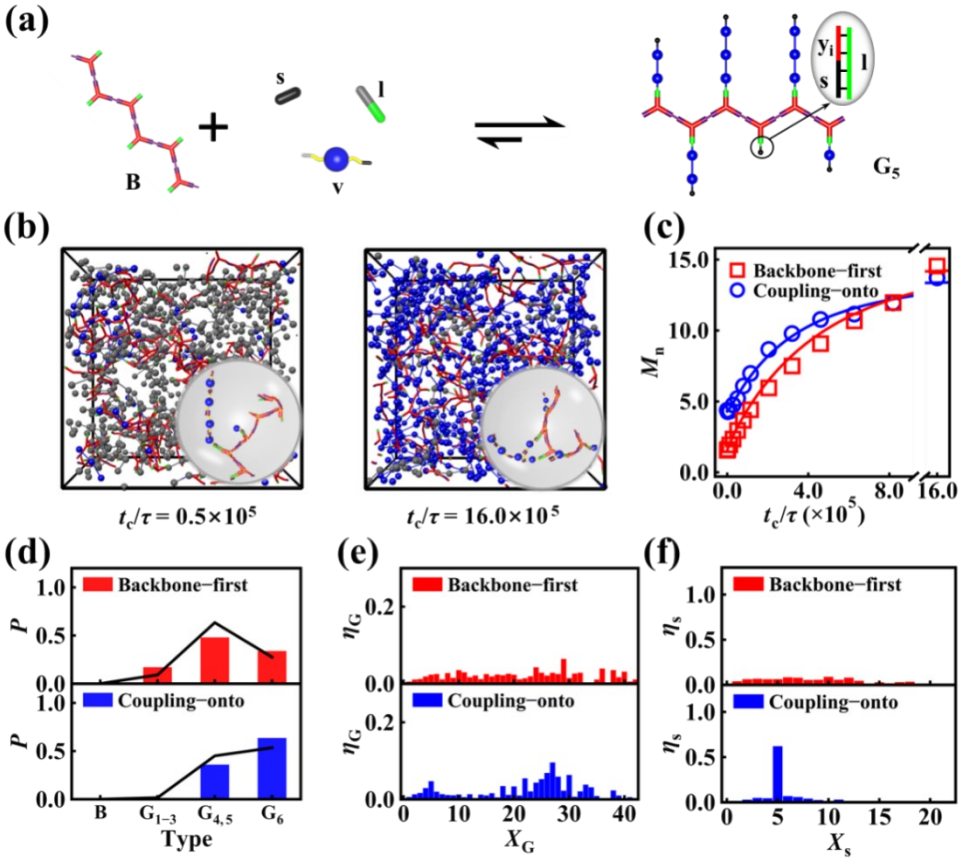

Fig. S18: Graft nanocopolymers constructed from backbone-first protocol. (a) Schematic drawing of the construction of graft nanocopolymers. Starting from active sites of backbones **B**, *bivalent DNA-NPs* **v** *polymerize into the sidechains of graft nanocopolymers in the presence of DNA linkers* **l** *and stoppers* **s**. *(b) Snapshots of coassembled nanostructures. The free prepolymers are represented by the gray color. (c) Temporal evolution of number-average degree M_n of polymerization under the backbone-first and coupling-onto protocols. (d) Number fraction P of free backbones* **B** *and graft nanocopolymers* $\mathbf{G_{ns}}$ *with various numbers n_s of graft sidechains. (e) Number fraction η_G of graft nanocopolymers as a function of their polymerization degree X_G of coassemblies. (f) Number fraction η_s of graft sidechains as a function of the length X_s of sidechains.*

S5.5 Gyration radius of graft nanocopolymers

Figure S19a shows the dependence of gyration radius $\langle R_g^2 \rangle^{1/2}$ of graft nanocopolymers on the length X_b of backbones. In general, the size of graft nanocopolymers satisfies the relationship of $\langle R_g^2 \rangle^{1/2} \sim X_b^{\gamma}$, where the scaling index γ is found to be dependent of the length X_s of graft sidechains. An increase of X_s results in a configuration transition of graft nanocopolymers from a coil-like shape to an elongated state (Figure S19b), corresponding to a change of scaling index from 0.60 to 0.20.

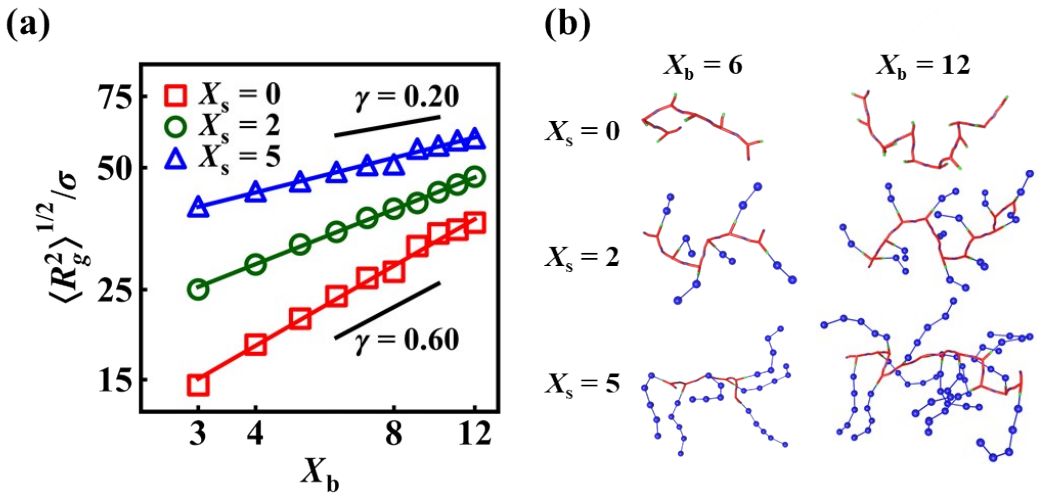

Fig. S19: (a) Double-logarithmic plot of gyration radius $\langle R_g^2 \rangle^{1/2}$ of graft nanocopolymers versus the length X_b of backbones under various length X_s of graft sidechains. (b) Conformations of graft nanocopolymers under various combinations of X_s and X_b.

S6. Additional figures for organizing DNA-NPs into different nanoarchitectures

The coupling-onto coassembly protocol can be applied to construct the miktoarm star nanocopolymers and star nanopolymers with higher functionality. Figure S20 shows the temporal change of the number-average degree M_n of polymerization and the number fraction P of distinct coassemblies with star nanoarchitecture. The formation of such star nanopolymers can be also captured by the coassembly kinetics model proposed in Subsection S2.2. Through the coupling-onto coassembly protocol, the DNA-based multicomponent mixture produces star nanopolymers with higher yield.

The coupling-onto coassembly protocol of DNA-based multicomponent mixture can also be extended to enable the realization of dendrimer-like superstructures, which is schematically illustrated in Figure S21a. The dendritic cores are assembled by the ligation of Y-shaped DNA motifs with specifically designed sequences of sticky ends (denoted as $\mathbf{Y_0}$, $\mathbf{Y_1}$ and $\mathbf{Y_2}$). One $\mathbf{Y_0}$ is linked with three $\mathbf{Y_1}$, forming first-generation dendrimer-like cores ($\mathbf{D_1}$). Subsequently, $\mathbf{D_1}$ is ligated to six $\mathbf{Y_2}$, resulting in second-generation dendrimer-like cores ($\mathbf{D_2}$). Note that the assembled $\mathbf{D_2}$ has 12 active sites, which are demonstrated by the coarse-grained simulations (Figure S21b). Lastly, the formed cores $\mathbf{D_2}$ mix with the prepolymers **V** to coassemble into the dendritic nanopolymers (Figure S21c).

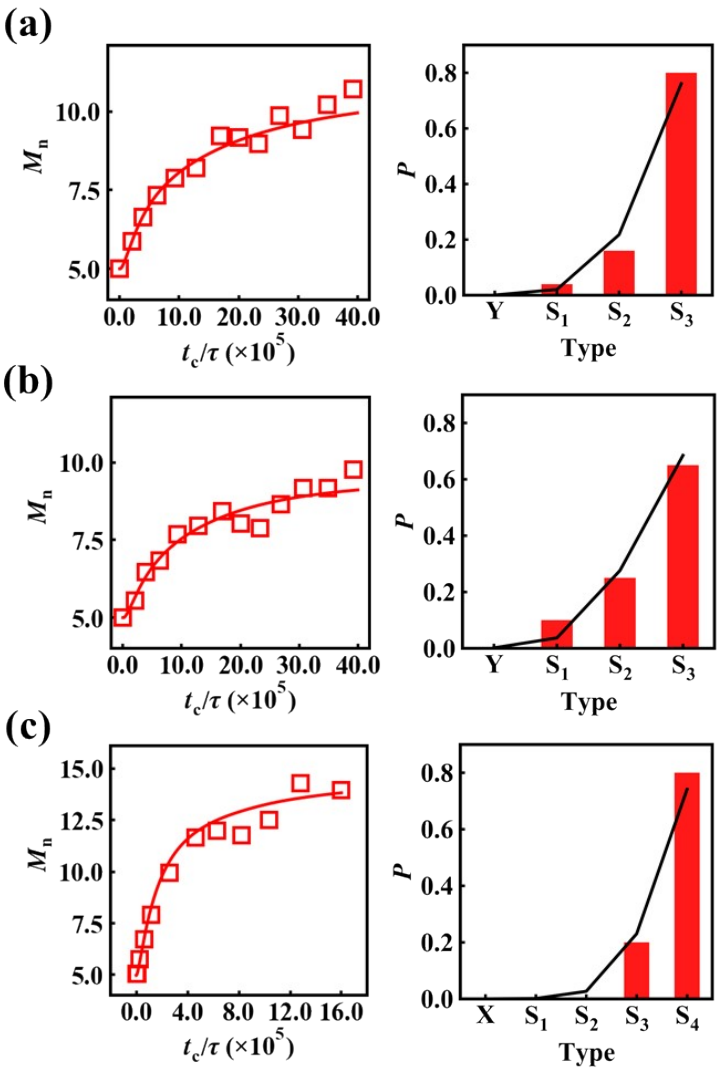

Fig. S20: (a-c) Coassembly of branch-shaped motifs **Y** *and end-capped prepolymers* **Y** *into (a) miktoarm star nanocopolymers having distinct composition of arms, (b) miktoarm star nanocopolymers having distinct length of arms and (c) regular star nanopolymers with four functionalities. (Left) Number-average degree* M_n *of polymerization as a function of the coassembly time* t_c*. (Right) Number fraction P of free branch-shaped motifs* **Y** *and star nanopolymers* **S***. The solid lines correspond to the numerical solutions of the theoretical model.*

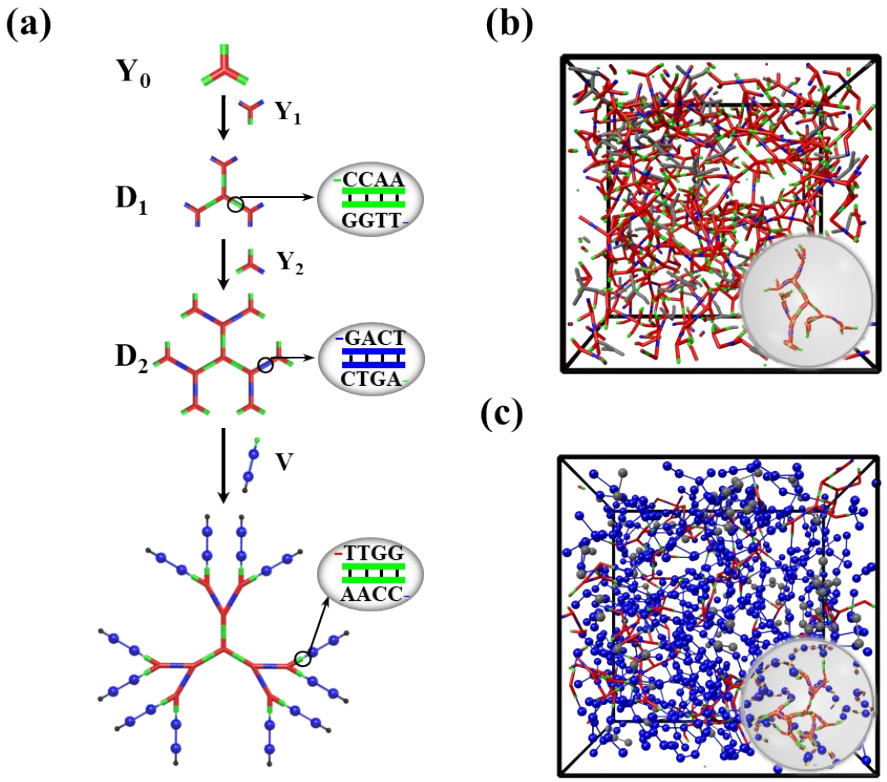

Fig. S21: (a) Schematic illustration of the construction of dendritic nanopolymers. Insets show the sequence and hybridization of DNA strands for the linkage of building units. (b) Typical conformation of coassembled assembled $\mathbf{D_2}$*. (c) Typical conformation of dendritic nanopolymers.*

REFERENCES

(S1) C. Knorowski, S. Burleigh and A. Travesset, *Phys. Rev. Lett.*, 2011, **106**, 215501.

(S2) C. Knorowski and A. Travesset, *J. Am. Chem. Soc.*, 2014, **136**, 653–659.

(S3) J. A. Anderson, C. D. Lorenz and A. Travesset, *J. Comput. Phys.*, 2008, **227**, 5342–5359.

(S4) J. Glaser, T. D. Nguyen, J. A. Anderson, P. Lui, F. Spiga, J. A. Millan, D. C. Morse and S. C. Glotzer, *Comput. Phys. Commun.*, 2015, **192**, 97–107.

(S5) T. I. N. G. Li, R. Sknepnek and M. Olvera de la Cruz, *J. Am. Chem. Soc.*, 2013, **135**, 8535–8541.

(S6) W. Humphrey, A. Dalke and K. Schulten, *J. Mol. Graph.*, 1996, **14**, 33–38.

(S7) M. Gu, X. Ma, L. Zhang and J. Lin, *J. Am. Chem. Soc.*, 2019, **141**, 16408–16415.
(S8) T. Cai, S. Zhao, J. Lin and L. Zhang, *ACS Nano*, 2022, **16**, 15907–15916.
(S9) P. J. Flory, *Principles of polymer chemistry*, Cornell University Press, Ithaca, New York, 1953.
(S10) A. Klinkova, H. Thérien-Aubin, R. M. Choueiri, M. Rubinstein and E. Kumacheva, *Proc. Natl. Acad. Sci.*, 2013, **110**, 18775–18779.
(S11) R. Jin, G. Wu, Z. Li, C. A. Mirkin and G. C. Schatz, *J. Am. Chem. Soc.*, 2003, **125**, 1643–1654.
(S12) S. Y. Park, A. K. R. Lytton-Jean, B. Lee, S. Weigand, G. C. Schatz and C. A. Mirkin, *Nature*, 2008, **451**, 553–556.
(S13) W. B. Rogers, W. M. Shih and V. N. Manoharan, *Nat. Rev. Mater.*, 2016, **1**, 16008.
(S14) G. Zhu, Z. Xu, Y. Yang, X. Dai and L.-T. Yan, *ACS Nano*, 2018, **12**, 9467–9475.
(S15) P. G. Gennes, *Scaling concepts in polymer physics*, Cornell University Press, Ithaca, New York, 1979.
(S16) M. Rubinstein and R. H. Colby, *Polymer Physics*, Oxford University Press, 2003.
(S17) M. Daoud and J. P. Cotton, *J. Phys.*, 1982, **43**, 531–538.
(S18) L. A. Molina and J. J. Freire, *Macromolecules*, 1999, **32**, 499–505.
(S19) G. H. Fredrickson, *Macromolecules*, 1993, **26**, 2825–2831.
(S20) S. Morozova and T. P. Lodge, *ACS Macro Lett.*, 2017, **6**, 1274–1279.
(S21) I. Teraoka, *Polymer solutions: an introduction to physical properties*, John Wiley & Sons, New York, 2002.
(S22) B. H. Zimm and W. H. Stockmayer, *J. Chem. Phys.*, 1949, **17**, 1301–1314.
(S23) I. Teraoka, *Macromolecules*, 2004, **37**, 6632–6639.